

Dear Editor Ma:

Please find below our itemized responses to the reviewer's comments. We have addressed the comments raised by both reviewers, and incorporated them in the revised manuscript.

Thank you very much for your consideration.

Sincerely,  
Lin Zhang, et al.

---

### **Anonymous Referee #2**

#### **Comment:**

This paper discussed atmospheric N deposition in the northeastern Pacific Ocean in relation to anthropogenic and natural reactive N emissions using the GEOS-chemical global chemistry model. The authors provided very important information on both dry and wet N deposition in Yellow Sea and South China Sea and compare their results with satellite data and emission inventory data with regional differences in anthropogenic reactive N sources. This is a significant contribution to scientific knowledge on how the terrestrial reactive N emissions affect N wet and dry deposition onto the northeastern Pacific Ocean (e.g. Yellow Sea and South China Seas).

#### **Response:**

**We thank the reviewer for the helpful comments. All of them have been addressed in the revised manuscript. Please see our itemized responses below.**

#### *Scientific comments:*

The authors jointly used modeling tool, satellite observation and surface measurement to obtain relatively accurate and comprehensive information on atmospheric nitrogen deposition to the northwestern Pacific, especially the China Seas. The results of this study contribute to a better understanding of coastal atmospheric N deposition and help to make effective strategies for mitigating N deposition. To further improve the quality of the manuscript, I suggest that a section of the uncertainty analysis (as also mentioned in later) may be presented in the text.

#### **Response:**

**We have added the following paragraphs in the conclusion section to discuss the main uncertainties.**

**“While this study provides a pilot investigation of the sources and processes controlling atmospheric nitrogen deposition to the northwestern Pacific, some uncertainties still need to be considered. A main uncertainty is associated with the lack of in-situ measurements to evaluate the model simulated nitrogen dry deposition fluxes. Uncertainties exist in both model calculated dry deposition velocities over the ocean surface (as discussed in section 2.1) and simulated surface concentrations of nitrogen species. Recent studies have shown that GEOS-Chem overestimates wintertime surface concentrations of nitrate and nitric acid (Heald et al., 2012; Zhang et al., 2012; Wang et al., 2013), which can**

lead to a model overestimation of NO<sub>y</sub> dry deposition flux in winter.

Uncertainties also exist in Asian NH<sub>3</sub> emissions; in particular, air-surface bi-directional NH<sub>3</sub> fluxes are not considered in the study. Although it has little impact on the oceanic emissions, recent implementations of the bi-directional NH<sub>3</sub> flux on fertilizer use showed lower NH<sub>3</sub> agricultural emissions over China (Fu et al., 2015; Zhu et al., 2015), and thus would lower its transport to the ocean. In addition, any bias in the GEOS-Chem simulation would affect the adjoint sensitivity. Also to ascribe nitrogen deposition to sources from different emission sectors, we rely on the bottom-up sectorial emissions to separate the adjoint sensitivity. Even though the total emissions can be constrained with the satellite measurements, the sectorial information is subject to larger uncertainties (Zhang et al., 2009). We recommend future research to reduce these uncertainties.”

Those references were added:

Fu, X., Wang, S. X., Ran, L. M., Pleim, J. E., Cooter, E., Bash, J. O., Benson, V., and Hao, J. M.: Estimating NH<sub>3</sub> emissions from agricultural fertilizer application in China using the bi-directional CMAQ model coupled to an agro-ecosystem model, *Atmos. Chem. Phys.*, 15, 6637-6649, 10.5194/acp-15-6637-2015, 2015.

Heald, C. L., Collett, J. L., Lee, T., Benedict, K. B., Schwandner, F. M., Li, Y., Clarisse, L., Hurtmans, D. R., Van Damme, M., Clerbaux, C., Coheur, P. F., Philip, S., Martin, R. V., and Pye, H. O. T.: Atmospheric ammonia and particulate inorganic nitrogen over the United States, *Atmos. Chem. Phys.*, 12, 10295-10312, 2012.

Wang, Y., Zhang, Q. Q., He, K., Zhang, Q., and Chai, L.: Sulfate-nitrate-ammonium aerosols over China: response to 2000-2015 emission changes of sulfur dioxide, nitrogen oxides, and ammonia, *Atmos. Chem. Phys.*, 13, 2635-2652, 2013.

Zhu, L., Henze, D., Bash, J., Jeong, G.-R., Cady-Pereira, K., Shephard, M., Luo, M., Paulot, F., and Capps, S.: Global evaluation of ammonia bi-directional exchange, *Atmos. Chem. Phys. Discuss.*, 15, 4823-4877, doi:10.5194/acpd-15-4823-2015, 2015.

*Technical corrections/Comments*

**Comment:**

Introduction Page13660. Line 7. The formation of ammonium particles increases . . .

**Response: Changed as suggested.**

**Comment:**

Page13660. Line 8. As dry removal of the particles . . .

**Response: We changed to “As dry removal of particles is slow”**

**Comment:**

Sect. 2.1 General description Page 13662. Lines 10, 15.

The monthly dry deposition velocities of Nr species (e.g. NO<sub>2</sub> and NH<sub>3</sub>) over the northwestern Pacific and seasonality of them differ from the results reported by Zhang et al. (2010) over the China Seas. Did this study consider impact of the sea-surface height on the velocities? How is the reliability if using the current deposition

velocities to the China Seas?

Reference mentioned: Zhang Y., et al. Atmospheric deposition of inorganic nitrogen to the eastern China seas and its implications to marine biogeochemistry. *Journal of Geophysical Research*, Vol. 115, D00K10, doi: 10.1029/2009JD012814, 2010.

**Response:**

**We now state in the text “For gaseous NH<sub>3</sub> and HNO<sub>3</sub>, Zhang et al. (2010) estimated similar dry deposition velocities (0.5-0.85 cm s<sup>-1</sup>) over the eastern China seas in spring-fall using the MM5/CMAQ model, but suggested minimum deposition velocities in winter (~0.5 cm s<sup>-1</sup> versus 1.10-1.16 cm s<sup>-1</sup> in our estimates). Understanding this discrepancy would require a close examination of differences between the two studies, such as different simulation years and different air-sea roughness parameterizations in the two models. Zhang et al. (2010) modified the sea-surface roughness length by considering the impact of sea-surface height, while GEOS-5 used in this study follows the Monin-Obhukov similarity theory with improved parameters to match recent air-sea exchange observations (Garfinkel et al., 2011).”**

**Added references:**

**Zhang, Y., Yu, Q., Ma, W. C., and Chen, L. M.: Atmospheric deposition of inorganic nitrogen to the eastern China seas and its implications to marine biogeochemistry, *J. Geophys. Res.-Atmos.*, 115, D00K10, 2010.**

**Garfinkel, C. I., Molod, A. M., Oman, L. D., and Song, I. S.: Improvement of the GEOS-5 AGCM upon updating the air-sea roughness parameterization, *Geophys. Res. Lett.*, 38, L18702, 2011.**

**Comment:**

3 Column concentrations and wet deposition fluxes over Asia

Page 13667. Line 5. The highest sensitivities

**Response: Changed as suggested (Added ‘the’).**

**Comment:**

Page 13668. Line 5.

This study shows that Annually model simulated nitrogen wet deposition (NH<sub>4</sub><sup>+</sup> + NO<sub>3</sub><sup>-</sup>) fluxes over China averages 9.3 kg N ha<sup>-1</sup> a<sup>-1</sup> with NH<sub>4</sub><sup>+</sup> contributing 70 %. However, this modeled magnitude of wet deposition was 1.6-times lower than the results reported by recent studies (Jia et al., 2014, 13.9 kg N ha<sup>-1</sup> a<sup>-1</sup>; Zhu et al., 2015, 13.2 kg N ha<sup>-1</sup> a<sup>-1</sup>) based on published large amount of Chinese surface measurements. In addition, although the contribution of NH<sub>4</sub><sup>+</sup> to total wet N deposition (70%) was similar to that in north China (Pan et al., 2012, in the range of 63-78%), it might be overestimated at the national scale as an average value of 55% has been observed by Zhu et al. (2015) based on 41 in situ monitoring sites across China. Therefore, the modeled flux of wet deposition may have some uncertainties. Please make a comprehensive comparison in the text.

References mentioned:

Jia, Y. L. et al., 2014. Spatial and decadal variations in inorganic nitrogen wet deposition in China induced by human activity. *Sci. Rep.*, 4, 3763.

Pan, Y. P. et al. 2012. Wet and dry deposition of atmospheric nitrogen at ten sites in Northern China. *Atmos. Chem. Phys.*, 12, 6515-6535.

Zhu, J. X. et al., 2015. The composition, spatial patterns, and influencing factors of atmospheric wet nitrogen deposition in Chinese terrestrial ecosystems. *Sci. Total Environ.*, 511, 777-785.

**Response:**

**We now add in the text: “Compared with previous studies using ensembles of surface measurements, our estimated annual nitrogen wet deposition over China is ~30% lower than the estimates of 13.9 kg N ha<sup>-1</sup> a<sup>-1</sup> by Jia et al. (2014) and 13.2 kg N ha<sup>-1</sup> a<sup>-1</sup> by Zhu et al. (2015), but is consistent with 9.88 kg N ha<sup>-1</sup> a<sup>-1</sup> by Lv and Tian (2007). The NH<sub>4</sub><sup>+</sup> contribution to wet deposition is higher than that estimated by Zhu et al. (2015) (55%), but is consistent with Lv and Tian (2007) (72%) and Pan et al. (2012) (63-78% over North China).**

**Added reference:**

**Jia, Y., Yu, G., He, N., Zhan, X., Fang, H., Sheng, W., Zuo, Y., Zhang, D., and Wang, Q.: Spatial and decadal variations in inorganic nitrogen wet deposition in China induced by human activity, *Scientific reports*, 4, 3763, 10.1038/srep03763, 2014.**

**Zhu, J., He, N., Wang, Q., Yuan, G., Wen, D., Yu, G., and Jia, Y.: The composition, spatial patterns, and influencing factors of atmospheric wet nitrogen deposition in Chinese terrestrial ecosystems, *Sci. Total Environ.*, 511, 777-785, 2015.**

**Comment:** Page 13668. Line 5. are greater than 0.7.

**Response:** Changed as suggested (changed ‘great’ to ‘greater’).

**Comment:**

Page 13668. Lines 7-8.

This is similar to Lv et al. (2007) who estimated . . .

**Response:** This has been changed according to an earlier comment.

**Comment:**

4.1 Seasonal variation and deposition process

Page 13669. Line 25. Accounting to Zhang et al. (2012), there were some uncertainties on seasonal amounts of NO<sub>y</sub> deposition modeled by Geos-Chem. Does this affect the current findings? Please clarify.

Reference mentioned: Zhang, L., et al. 2012. Nitrogen Deposition to the United States: Distribution, Sources, and Processes, *Atmos. Chem. Phys.*, 12, 4539-4554.

**Response:**

**This has been addressed in replying the earlier comment on uncertainties.**

**We added in the text “Recent studies have shown that GEOS-Chem overestimates wintertime surface concentrations of nitrate and nitric acid (Heald et al., 2012; Zhang et al., 2012; Wang et al., 2013), which can lead to a model overestimation of NO<sub>y</sub> dry deposition flux in winter.”**

**Comment:**

Page 13670. Lines 1-2. higher than in April and July

**Response:**

**Changed as suggested (added 'in').**

**Comment:**

Page 13671. Line 10. Spatial and seasonal variations of atmospheric nitrogen...

**Response:**

**Changed as suggested (changed 'variation' to 'variations').**

---

**Anonymous Referee #3**

**Comment:**

This paper presents a calculation of the total nitrogen flux to the Yellow and South China Seas, and also determines contributions from various emission source categories to that flux. It appears to be a very thorough paper, and contributes to the further understanding of nitrogen deposition to oceans. It is well organized and well written and I recommend it be published in ACP, after addressing a few details below.

**Response:**

**We thank the reviewer for the helpful comments. All of them have been addressed in the revised manuscript. Please see our itemized responses below.**

**Comment:**

P 13659, L 1: I think you should be a bit more precise here, especially for the last line of your abstract, and which could have significant policy implications. Maybe change to "limiting the effectiveness of NH<sub>3</sub> emission controls on reducing nitrogen deposition to the Yellow and South China Seas". At first glance it reads like reducing NH<sub>3</sub> isn't useful at all

**Response:**

**As suggested, we changed this sentence to "limiting the effectiveness of NH<sub>3</sub> emission controls on reducing nitrogen deposition to the Yellow Sea."**

**Comment:**

P 13660, L 10: If 40% enters ocean, does other 60% end up on land generally? (Ie, is this global?)

**Response:**

**Yes, we modified the sentence to "Globally a large fraction (~40%) of emitted NH<sub>3</sub> and NO<sub>x</sub> enters the ocean via wet and dry deposition from the atmosphere, and the rest ~60% is deposited over the land (Duce et al., 2008)."**

**Comment:**

P 13663: I believe nighttime GEOS mixed layer depth in this version of GEOS-Chem had some problems. What do you do for mixed layer depth? Does it influence the results at all?

**Response:**

The PBL problem has been corrected in our simulations.

We added in the model description section 2.1 “The GEOS-5 data have a low bias for nighttime planetary boundary layer height (PBLH). This has been corrected by setting a minimum PBLH computed as a function of local friction velocity (Koracin and Berkowicz, 1988; Sajeev Philip; [http://wiki.seas.harvard.edu/geos-chem/index.php/Boundary\\_layer\\_mixing](http://wiki.seas.harvard.edu/geos-chem/index.php/Boundary_layer_mixing)).”.

**Added references**

**Koracin, D., and Berkowicz, R.: Nocturnal boundary-layer height: Observations by acoustic sounders and predictions in terms of surface-layer parameters, *Boundary-Layer Meteorol.*, 43, 65-83, 1988.**

**Comment:**

You mention NH<sub>3</sub> from the oceans here and then later in text/figures, but for the meantime, it would be nice to get an idea of the magnitude of NH<sub>3</sub> oceanic emissions when you are discussing N emissions from Asia. What fraction of the total natural NH<sub>3</sub> is from the oceans? (Maybe I missed this.)

**Response:**

We now state in the text “42% of the natural NH<sub>3</sub> emissions are from the oceanic emissions (0.50 Tg N a<sup>-1</sup>) over the region.” We have also listed the value (0.50 Tg N a<sup>-1</sup>) in Table 2.

**Comment:**

I don't believe GEOS-Chem has bidirectional exchange in the model, which may cause uncertainties in net flux for certain nitrogen species. Will this influence ocean estimates at all?

**Response:**

We have added in the section 2.2 (emissions) “Here we have not considered air-surface bi-directional exchange of NH<sub>3</sub> (Sutton et al., 1998), and treat the NH<sub>3</sub> fluxes as uncoupled emission and deposition processes.”.

We also state in the conclusion “Uncertainties also exist in Asian NH<sub>3</sub> emissions; in particular, air-surface bi-directional NH<sub>3</sub> fluxes are not considered in the study. Although it has little impact on the oceanic emissions, recent implementations of the bi-directional NH<sub>3</sub> flux on fertilizer use showed lower NH<sub>3</sub> agricultural emissions over China (Fu et al., 2015; Zhu et al., 2015), and thus would lower its transport to the ocean.”.

**Added references:**

**Fu, X., Wang, S. X., Ran, L. M., Pleim, J. E., Cooter, E., Bash, J. O., Benson, V., and Hao, J. M.: Estimating NH<sub>3</sub> emissions from agricultural fertilizer application in China using the bi-directional CMAQ model coupled to an agro-ecosystem model, *Atmos. Chem. Phys.*, 15, 6637-6649, 10.5194/acp-15-6637-2015, 2015.**

**Sutton, M. A., Burkhardt, J. K., Guerin, D., Nemitz, E., and Fowler, D.: Development of resistance models to describe measurements of bi-directional**

ammonia surface-atmosphere exchange, *Atmos. Environ.*, **32**, 473–480, 1998.  
Zhu, L., Henze, D., Bash, J., Jeong, G.-R., Cady-Pereira, K., Shephard, M., Luo, M., Paulot, F., and Capps, S.: Global evaluation of ammonia bi-directional exchange, *Atmos. Chem. Phys. Discuss.*, **15**, 4823-4877, doi:10.5194/acpd-15-4823-2015, 2015.

**Comment:**

Satellite data: Can you be a bit more specific about what exactly you are trying to achieve with this satellite validation? A spatial validation of GEOS-Chem NO<sub>x</sub> emissions? Since NO<sub>2</sub> has such a small deposition velocity, why care about NO<sub>2</sub>?

**Response:**

We now state in the text “Figure 2 compares GEOS-Chem simulated NH<sub>3</sub> and NO<sub>2</sub> tropospheric columns with satellite measurements. These comparisons provide valuable tests of the nitrogen emissions and their spatial distributions in the model since both NH<sub>3</sub> and NO<sub>2</sub> have short lifetimes in the atmosphere. Although NO<sub>2</sub> has a small dry deposition velocity (Table 1), it rapidly converts to other NO<sub>y</sub> species, thus NO<sub>2</sub> emissions still largely control the deposition of NO<sub>y</sub>.”

**Comment:**

There have been lots of OMI NO<sub>2</sub> comparisons with models. Maybe list if there are DOMINO NO<sub>2</sub> and GEOS-Chem papers already published, or at least DOMINO NO<sub>2</sub> validation to show OMI is useful.

**Response:**

We state in the text “The DOMINO NO<sub>2</sub> data has been validated against surface and aircraft observations (Boersma et al., 2008; 2009; Hains et al., 2010), and used to constrain NO<sub>x</sub> emissions in the model (Boersma et al., 2008; Lamsal et al., 2010).”

**Added references:**

Boersma, K. F., Jacob, D., Bucsel, E., Perring, A., Dirksen, R., van der A, R., Yantosca, R., Park, R., Wenig, M., Bertram, T., and Cohen, R.: Validation of OMI tropospheric NO<sub>2</sub> observations during INTEX-B and application to constrain NO<sub>x</sub> emissions over the eastern United States and Mexico, *Atmos. Environ.*, **42**(19), 4480–4497, 2008.

Boersma, K. F., Jacob, D. J., Trainic, M., Rudich, Y., DeSmedt, I., Dirksen, R., and Eskes, H. J.: Validation of urban NO<sub>2</sub> concentrations and their diurnal and seasonal variations observed from the SCIAMACHY and OMI sensors using in situ surface measurements in Israeli cities, *Atmos. Chem. Phys.*, **9**, 3867-3879, doi:10.5194/acp-9-3867-2009, 2009.

Hains, J. C., Boersma, K., Kroon, M., Dirksen, R., Cohen, R., Perring, A., Bucsel, E., Volten, H., Swart, D., Richter, A., Wittrock, F., Schoenhardt, A., Wagner, T., Ibrahim, O., van Roozendaal, M., Pinardi, G., Gleason, J., Veefkind, P., and Levelt, P.: Testing and Improving OMI DOMINO Tropospheric NO<sub>2</sub> Using Observations from the DANDELIONS and INTEXB Validation Campaigns, *J. Geophys. Res.*, **115**, D05301, doi:10.1029/2009JD012399, 2010.

Lamsal, L. N., Martin, R. V., van Donkelaar, A., Celarier, E. A., Bucsel, E. J.,

**Boersma, K. F., Dirksen, R., Luo, C., and Wang, Y.: Indirect validation of tropospheric nitrogen dioxide retrieved from the OMI satellite instrument: Insight into the seasonal variation of nitrogen oxides at northern midlatitudes, J. Geophys. Res., 115, D05302, 10.1029/2009jd013351, 2010.**

**Comment:**

Have you used the OMI scattering weights (column averaging kernels) to compare with the model? Huijnen et al 2010 showed the kind of differences that ignoring these can cause in model comparisons (Huijnen et al. "Comparison of OMI NO<sub>2</sub> tropospheric columns with an ensemble of global and European regional air quality models." Atmospheric Chemistry and Physics 10.7 (2010): 3273-3296.)

**Response:**

**We now state in the text “Recent studies have indicated that DOMINO NO<sub>2</sub> columns might be biased high due to the a priori profile shape, error in the surface air-mass factor, and exclusion of aerosols in the retrieval (Hains et al., 2010; Lamsal et al., 2010; Lin et al., 2014). The comparison also did not apply the averaging kernels to the model simulated columns, which may lead to additional biases when simulated NO<sub>2</sub> vertical profiles are different from the a priori profiles used in the OMI retrievals (Huijnen et al., 2010).”**

**Add the following reference:**

**Huijnen, V., Eskes, H. J., Poupkou, A., Elbern, H., Boersma, K. F., Foret, G., Sofiev, M., Valdebenito, A., Flemming, J., Stein, O., Gross, A., Robertson, L., D'Isidoro, M., Kioutsioukis, I., Friese, E., Amstrup, B., Bergstrom, R., Strunk, A., Vira, J., Zyryanov, D., Maurizi, A., Melas, D., Peuch, V. H., and Zerefos, C.: Comparison of OMI NO<sub>2</sub> tropospheric columns with an ensemble of global and European regional air quality models, Atmos. Chem. Phys., 10, 3273-3296, 2010.**

**Comment:**

Why is OMI data not treated as TES data and matched to GEOS-Chem coincidence along track? Do you expect any kind of bias might result? What is the cloud filtering criterion for these data?

**Response:**

**We now state in the text “The GEOS-Chem model results for 2009 are sampled along the TES orbit tracks at the overpass time (the standard TES products are level-2 data due to the sparse daily spatial coverage)” and “we filter the TES observations based on the retrieval quality control flags, and only use the daytime observations with cloud optical depth < 1.0.”**

**For OMI, we now state “To facilitate the comparison we use the monthly gridded tropospheric NO<sub>2</sub> column data which are averages of the retrievals with cloud radiance fraction < 50% ([http://www.temis.nl/docs/readme\\_tomsascii.pdf](http://www.temis.nl/docs/readme_tomsascii.pdf))”**

**Comment:**

There's not much discussion of uncertainties in the paper. I'm mostly wondering



about the adjoint. Is there a way to estimate uncertainties in these contribution estimates?

**Response:**

**We have added the following paragraphs to discuss uncertainties of the study, including uncertainty from the adjoint source contribution.**

**“While this study provides a pilot investigation of the sources and processes controlling atmospheric nitrogen deposition to the northwestern Pacific, some uncertainties still need to be considered. A main uncertainty is associated with the lack of in-situ measurements to evaluate the model simulated nitrogen dry deposition fluxes. Uncertainties exist in both model calculated dry deposition velocities over the ocean surface (as discussed in section 2.1) and simulated surface concentrations of nitrogen species. Recent studies have shown that GEOS-Chem overestimates wintertime surface concentrations of nitrate and nitric acid (Heald et al., 2012; Zhang et al., 2012; Wang et al., 2013), which can lead to a model overestimation of  $\text{NO}_y$  dry deposition flux in winter.**

**Uncertainties also exist in Asian  $\text{NH}_3$  emissions; in particular, air-surface bi-directional  $\text{NH}_3$  fluxes are not considered in the study. Although it has little impact on the oceanic emissions, recent implementations of the bi-directional  $\text{NH}_3$  flux on fertilizer use showed lower  $\text{NH}_3$  agricultural emissions over China (Fu et al., 2015; Zhu et al., 2015), and thus would lower its transport to the ocean. In addition, any bias in the GEOS-Chem simulation would affect the adjoint sensitivity. Also to ascribe nitrogen deposition to sources from different emission sectors, we rely on the bottom-up sectorial emissions to separate the adjoint sensitivity. Even though the total emissions can be constrained with the satellite measurements, the sectorial information is subject to larger uncertainties (Zhang et al., 2009). We recommend future research to reduce these uncertainties.”**

**Added references:**

**Heald, C. L., Collett, J. L., Lee, T., Benedict, K. B., Schwandner, F. M., Li, Y., Clarisse, L., Hurtmans, D. R., Van Damme, M., Clerbaux, C., Coheur, P. F., Philip, S., Martin, R. V., and Pye, H. O. T.: Atmospheric ammonia and particulate inorganic nitrogen over the United States, *Atmos. Chem. Phys.*, 12, 10295-10312, 2012.**

**Wang, Y., Zhang, Q. Q., He, K., Zhang, Q., and Chai, L.: Sulfate-nitrate-ammonium aerosols over China: response to 2000-2015 emission changes of sulfur dioxide, nitrogen oxides, and ammonia, *Atmos. Chem. Phys.*, 13, 2635-2652, 2013.**

**Minor comments:**

P13658, L 15: Change “downwind the Asian” to “downwind of the Asian”

P13659, L 8: Remove word “But” (never start a formal sentence with but).

P13659, L 24: You are not really addressing the issue (that’s for policy makers).

Change “address” to “study”

**Response:**

**Those comments are all changed as suggested.**

1  
2  
3  
4  
5  
6  
7  
8  
9  
10  
11  
12  
13  
14  
15  
16  
17  
18  
19  
20  
21

**Atmospheric nitrogen deposition to the northwestern Pacific: seasonal variation and source attribution**

Yuanhong Zhao<sup>1</sup>, Lin Zhang<sup>1</sup>, Yuepeng Pan<sup>2</sup>, Yuesi Wang<sup>2</sup>, Fabien Paulot<sup>3</sup>, Daven K. Henze<sup>4</sup>

[1] {Laboratory for Climate and Ocean-Atmosphere Sciences, Department of Atmospheric and Oceanic Sciences, School of Physics, Peking University, Beijing 100871, China}

[2] {State Key Laboratory of Atmospheric Boundary Layer Physics and Atmospheric Chemistry (LAPC), Institute of Atmospheric Physics, Chinese Academy of Sciences, Beijing 100029, China}

[3] {Program in Atmospheric and Oceanic Sciences, Princeton University, Princeton, New Jersey 08540, United States}

[4]{Department of Mechanical Engineering, University of Colorado, Boulder, Colorado 80309, United States}

Correspondence to Lin Zhang ([zhanglg@pku.edu.cn](mailto:zhanglg@pku.edu.cn))

22 **Abstract**

23 Rapid Asian industrialization has led to increased atmospheric nitrogen deposition  
24 downwind threatening the marine environment. We present an analysis of the sources  
25 and processes controlling atmospheric nitrogen deposition to the northwestern Pacific,  
26 using the GEOS-Chem global chemistry model and its adjoint model at  $1/2^\circ \times 2/3^\circ$   
27 horizontal resolution over the East Asia and its adjacent oceans. We focus our  
28 analyses on the marginal seas: the Yellow Sea and the South China Sea. Asian  
29 nitrogen emissions in the model are  $28.6 \text{ Tg N a}^{-1}$  as  $\text{NH}_3$  and  $15.7 \text{ Tg N a}^{-1}$  as  $\text{NO}_x$ .  
30 China has the largest sources with  $12.8 \text{ Tg N a}^{-1}$  as  $\text{NH}_3$  and  $7.9 \text{ Tg N a}^{-1}$  as  $\text{NO}_x$ ; the  
31 high  $\text{NH}_3$  emissions reflect its intensive agricultural activities. We find Asian  $\text{NH}_3$   
32 emissions are a factor of 3 higher in summer than winter. The model simulation for  
33 2008-2010 is evaluated with  $\text{NH}_3$  and  $\text{NO}_2$  column observations from satellite  
34 instruments, and wet deposition flux measurements from surface monitoring sites.  
35 Simulated atmospheric nitrogen deposition to the northwestern Pacific ranges  $0.8\text{-}20$   
36  $\text{kg N ha}^{-1} \text{ a}^{-1}$ , decreasing rapidly downwind of the Asian continent. Deposition fluxes  
37 average  $11.9 \text{ kg N ha}^{-1} \text{ a}^{-1}$  ( $5.0$  as reduced nitrogen  $\text{NH}_x$  and  $6.9$  as oxidized nitrogen  
38  $\text{NO}_y$ ) to the Yellow Sea, and  $5.6 \text{ kg N ha}^{-1} \text{ a}^{-1}$  ( $2.5$  as  $\text{NH}_x$  and  $3.1$  as  $\text{NO}_y$ ) to the  
39 South China Sea. Nitrogen sources over the ocean (ship  $\text{NO}_x$  and oceanic  $\text{NH}_3$ ) have  
40 little contribution to deposition over the Yellow Sea, about 7% over the South China  
41 Sea, and become important (greater than 30%) further downwind. We find that the  
42 seasonality of nitrogen deposition to the northwestern Pacific is determined by  
43 variations in meteorology largely controlled by the East Asian Monsoon and in  
44 nitrogen emissions. The model adjoint further estimates that nitrogen deposition to the  
45 Yellow Sea originates from sources over China (92% contribution) and the Korean  
46 peninsula (7%), and by sectors from fertilizer use (24%), power plants (22%), and  
47 transportation (18%). Deposition to the South China Sea shows source contribution  
48 from Mainland China (66%), Taiwan (20%), and the rest 14% from the Southeast  
49 Asian countries and oceanic  $\text{NH}_3$  emissions. The adjoint analyses also indicate that  
50 reducing Asian  $\text{NH}_3$  emissions would increase  $\text{NO}_y$  dry deposition to the Yellow Sea  
51 ( $28\%$  offset annually), limiting the effectiveness of  $\text{NH}_3$  emission controls on

52 | [reducing nitrogen deposition to the Yellow Sea.](#)

53

54 | **Keywords:** fixed nitrogen; nitrogen deposition; northwestern Pacific; adjoint

55

## 56 | 1 Introduction

57

58 | Anthropogenic emissions of reactive nitrogen (or fixed nitrogen) have led to a rapid  
59 | growth of nitrogen deposition to both land and marine ecosystems (Galloway et al.,  
60 | 2004; Duce et al., 2008; Liu et al., 2013). This additional input of nitrogen nutrient  
61 | may enhance the primary production and carbon storage of the terrestrial biosphere  
62 | (Pregitzer et al., 2008; Hyvonen et al., 2008). Excessive nitrogen deposition has been  
63 | observed over sensitive ecosystems and can cause adverse effects including soil  
64 | acidification and a reduction in plant biodiversity over land (Bowman et al., 2008;  
65 | Stevens et al., 2004), and eutrophication on lakes and oceans (Bouwman et al., 2002).

66

67 | The northwestern Pacific is a region vulnerable to atmospheric nitrogen deposition as  
68 | its productivity is generally limited by the low nutrient supply from deep water (Duce  
69 | et al., 2008; Kim et al., 2011; 2014). Frequent incidences of harmful algal blooms in  
70 | the marginal seas of the Pacific Ocean such as the Yellow Sea have been of great  
71 | concern (Hu et al., 2010). This region is subject to significant anthropogenic nitrogen  
72 | deposition as it is located downwind of the Asian continent with high fixed nitrogen  
73 | emissions from increasing human activities (Kurokawa et al., 2013; Luo et al., 2014).  
74 | Increased nitrogen availability in waters of the northwestern Pacific has been  
75 | observed in the past 30 years, most likely due to increasing deposition from the  
76 | atmosphere (Kim et al., 2011). To alleviate the eutrophication conditions in the  
77 | northwestern Pacific requires a better understanding of the sources and atmospheric  
78 | processes controlling nitrogen deposition to the region. Here we use a nested global  
79 | chemical transport model (GEOS-Chem) and its adjoint to [study](#) the issue.

80

81 | Atmospheric nitrogen deposition mainly originates from emissions of ammonia (NH<sub>3</sub>)

lin zhang 15/9/1 11:41 AM

已删除: But

lin zhang 15/9/1 11:41 AM

已删除: e

lin zhang 15/9/1 11:41 AM

已删除: address

85 and nitrogen oxides ( $\text{NO}_x \equiv \text{NO} + \text{NO}_2$ ).  $\text{NO}_x$  sources include fuel combustion,  
86 lightning, and microbial processes in soil. It can be oxidized to nitric acid ( $\text{HNO}_3$ ) and  
87 organic nitrates in the atmosphere on a time scale less than one day except in  
88 extratropical winter (1-2 days) (Martine et al., 2003).  $\text{HNO}_3$  is water-soluble and is  
89 readily removed from the atmosphere by both wet and dry deposition.  $\text{NH}_3$  is mainly  
90 produced by agricultural activities (fertilizer use and manure management), human  
91 waste, as well as natural sources such as oceanic emissions (Bouwman et al., 1997).  
92 Reacting with  $\text{H}_2\text{SO}_4$  and  $\text{HNO}_3$ ,  $\text{NH}_3$  forms ammonium sulfate and ammonium  
93 nitrate particles in the atmosphere. The formation of ammonium particles increases  
94 the lifetime of nitrogen in the atmosphere, promoting its long-range transport as dry  
95 removal of particles is slow.

lin zhang 15/9/1 11:06 AM

已删除: deposition

lin zhang 15/9/1 11:06 AM

已删除: for particles

96  
97 Globally a large fraction (~40%) of emitted  $\text{NH}_3$  and  $\text{NO}_x$  enters the ocean via wet  
98 and dry deposition from the atmosphere, and the rest ~60% is deposited over the land  
99 (Duce et al., 2008). Inputs from rivers provide additional fixed nitrogen to the ocean,  
100 but it is estimated that much of the riverine nitrogen is lost by denitrification in  
101 continental shelves and has a smaller impact on the open ocean (Seitzinger et al., 2006;  
102 Duce et al., 2008). Sanderson et al. (2008) showed using multiple models that about  
103 10-15% of the emitted  $\text{NO}_x$  is exported out of East Asia as nitrogen oxides ( $\text{NO}_y \equiv$   
104  $\text{NO}_x + \text{HNO}_3 + \text{aerosol NO}_3^- + \text{PAN} + \text{N}_2\text{O}_5 + \text{isoprene nitrates}$ ) with 34%-49% of  
105 them deposited within 1000-km distance. A number of studies have examined the  
106 processes of Asian pollution transport to the Pacific (Liu et al., 2003; Liang et al.,  
107 2004; Dickerson et al., 2007). Few studies have been conducted to quantify the  
108 patterns, processes, and source attribution of atmospheric nitrogen deposition to the  
109 northwestern Pacific.

lin zhang 15/9/1 11:33 AM

已删除: A large fraction (~40%) of emitted  $\text{NH}_3$  and  $\text{NO}_x$  enters the ocean via wet and dry deposition from the atmosphere (Duce et al., 2008)

110  
111 We use the nested version of GEOS-Chem global chemical transport model (CTM)  
112 and its adjoint model with horizontal resolution of  $1/2^\circ \times 2/3^\circ$  (Chen et al., 2009; Jiang  
113 et al., 2015) to investigate the factors controlling atmospheric nitrogen deposition to  
114 the northwestern Pacific, particularly over the Yellow Sea and the South China Sea.

121 Three-year (2008-2010) GEOS-Chem model simulations are conducted to quantify  
122 the deposition processes and to understand the impact of meteorology on the seasonal  
123 variability of atmospheric deposition. We evaluate the model simulation with surface  
124 measurements of wet deposition fluxes and satellite observations of NH<sub>3</sub> and NO<sub>2</sub>  
125 columns. We further use the adjoint method to ascribe nitrogen deposition to the  
126 Yellow Sea and the South China Sea to nitrogen sources from different regions and  
127 sectors.

128

## 129 **2. The GEOS-Chem model and its adjoint**

### 130 **2.1 General description**

131

132 We use a nested version of the GEOS-Chem 3-D global CTM (Chen et al., 2009;  
133 Zhang et al., 2012; 2014; <http://geos-chem.org>) driven by GEOS-5 (Goddard Earth  
134 Observing System) assimilated meteorological data from NASA Global Modeling and  
135 Assimilation Office (GMAO). The GEOS-5 meteorological data have a temporal  
136 resolution of 6 hours (3 hours for surface variables and mixing layer depths), a  
137 horizontal resolution of 1/2° latitude × 2/3° longitude, and 72 layers in the vertical.  
138 We use the native 1/2°×2/3° horizontal resolution over the East Asia and its adjacent  
139 oceans (70°E-150°E, 11°S-55°N), and 4°×5° over the rest of the world. We present  
140 results from three-year GEOS-Chem simulations for 2008-2010. A global 4°×5°  
141 simulation is first conducted to provide the boundary conditions for the nested model  
142 at 3-h temporal resolution. Simulations are initialized on January 1, 2008 with model  
143 fields generated by a 6-month spin-up run at both 4°×5° and nested resolutions.

144

145 Zhang et al. (2012) has applied a similar nested model for North America to analyze  
146 the sources and processes of nitrogen deposition to the United States. The model  
147 includes a fully coupled tropospheric ozone-NO<sub>x</sub>-hydrocarbon-aerosol chemical  
148 mechanism (Bey et al., 2001; Park et al., 2004; Mao et al., 2010). Partitioning of gas  
149 and aerosol phase of total NH<sub>3</sub> and HNO<sub>3</sub> is calculated using the ISORROPIA II  
150 thermodynamic equilibrium model (Fountoukis and Nenes, 2007). Following Zhang

151 et al. (2012), we assume that isoprene nitrates produced from the oxidation of  
152 biogenic isoprene are removed by dry and wet deposition at the same rate as  $\text{HNO}_3$ .  
153 The reactive uptake coefficients for  $\text{N}_2\text{O}_5$  in aerosols are from Evans and Jacob  
154 (2005), but are reduced by a factor of 10 as in Zhang et al. (2012).

155

156 Model parameterization of wet deposition via both convective updraft and large-scale  
157 precipitation scavenging follows the scheme described by Liu et al. (2001) for aerosol,  
158 and by Mari et al. (2000) and Amos et al. (2012) for soluble gas. Dry deposition  
159 calculation follows a standard big-leaf resistance-in-series model (Wesely, 1989)  
160 including the aerodynamic resistance, the boundary layer resistance, and the canopy  
161 or surface uptake resistance. Dry deposition velocities are calculated relative to the  
162 lowest model layer (~70 m above the surface) as discussed in Zhang et al. (2012). [The  
163 GEOS-5 data have a low bias for nighttime planetary boundary layer height \(PBLH\).  
164 This has been corrected by setting a minimum PBLH computed as a function of local  
165 friction velocity \(Koracin and Bberkowicz, 1988; Sajeew Philip;  
166 \[http://wiki.seas.harvard.edu/geos-chem/index.php/Boundary\\\_layer\\\_mixing\]\(http://wiki.seas.harvard.edu/geos-chem/index.php/Boundary\_layer\_mixing\)\).](#)

167

168 Table 1 summarizes the model calculation of monthly mean daytime (10:00-16:00  
169 local time) dry deposition velocities for different nitrogen species over the  
170 northwestern Pacific. Calculated dry deposition velocities are largest for  $\text{HNO}_3$ ,  $\text{N}_2\text{O}_5$   
171 ( $0.56\text{-}1.16\text{ cm s}^{-1}$ ) and  $\text{NH}_3$  ( $0.60\text{-}1.10\text{ cm s}^{-1}$ ),  $0.06\text{-}0.08\text{ cm s}^{-1}$  for aerosol  $\text{NH}_4^+$  and  
172  $\text{NO}_3^-$ , and near zero for insoluble species such as  $\text{NO}_2$  and PAN. The values are  
173 generally much smaller than those over land (e.g., Table 1 of Zhang et al. (2012)) as  
174 the uptake resistance over the smooth ocean surface is high. Deposition velocities are  
175 higher in winter than those in summer due to stronger winds near the ocean surface in  
176 winter.

177

178 The model calculated dry deposition velocities for aerosols are consistent with the  
179 mean value of  $0.1\text{ cm s}^{-1}$  (with a range of  $0.03\text{-}0.3\text{ cm s}^{-1}$ ) estimated by Duce et al.  
180 (1991) for aerosol dry deposition over the ocean surface. [For gaseous  \$\text{NH}\_3\$  and  \$\text{HNO}\_3\$ ,](#)

181 Zhang et al. (2010) estimated similar dry deposition velocities (0.5-0.85 cm s<sup>-1</sup>) over  
182 the eastern China seas in spring-fall using the MM5/CMAQ model, but suggested  
183 minimum deposition velocities in winter (~0.5 cm s<sup>-1</sup> versus 1.10-1.16 cm s<sup>-1</sup> in our  
184 estimates). Understanding this discrepancy would require a close examination of  
185 differences between the two studies, such as different simulation years and different  
186 air-sea roughness parameterizations in the two models. Zhang et al. (2010) modified  
187 the sea-surface roughness length by considering the impact of sea-surface height,  
188 while GEOS-5 used in this study follows the Monin-Obhukov similarity theory with  
189 improved parameters to match recent air-sea exchange observations (Garfinkel et al.,  
190 2011).

191

## 192 **2.2 Emissions**

193

194 Global anthropogenic emissions (NO<sub>x</sub>, SO<sub>2</sub>, CO, and non-methane VOCs) are from  
195 the Emission Database for Global Atmospheric Research (EDGAR) inventory  
196 (Olivier and Berdowski, 2001) except for global anthropogenic NH<sub>3</sub> emissions that  
197 are taken from the Global Emissions Initiative (GEIA) inventory (Bouwman et al.,  
198 1997). Regional emission inventories are then applied including the European  
199 Monitoring and Evaluation Programme (EMEP) inventory (Vestreng and Klein, 2002)  
200 over Europe, the EPA 2005 National Emissions Inventory (NEI-2005) over the US,  
201 the Canada Criteria Air Contaminants (CAC) inventory  
202 (<http://www.ec.gc.ca/pollution/default.asp?lang=En&n=E96450C4-1>) over Canada,  
203 and the Regional Emission inventory in Asia (REAS-v2) inventory for 2008  
204 (Kurokawa et al., 2013) over Asia (with updates for NH<sub>3</sub> emissions as described  
205 below). Global ship NO<sub>x</sub> emissions are from the International Comprehensive  
206 Ocean–Atmosphere Data Set (ICOADS) (Wang et al., 2008). The emitted NO<sub>x</sub> from  
207 ships is directly converted into HNO<sub>3</sub> and ozone to account for their rapid chemistry  
208 at a sub-grid scale (Vinken et al., 2011).

209

210 The model also includes various natural sources of NH<sub>3</sub> and NO<sub>x</sub>. Lightning NO<sub>x</sub>



211 emissions are calculated using the cloud top height parameterization of Price and Rind  
212 (1992), vertically distributed following Pickering et al. (1998), and further spatially  
213 constrained with satellite observations as described by Sauvage (2007) and Murray et  
214 al. (2012). Global lightning source is adjusted to be 6 Tg N a<sup>-1</sup> (Martin et al., 2007).  
215 Soil emissions are computed by the algorithm Yienger and Levy (1995) with canopy  
216 reduction factors (Wang et al., 1998). Biomass burning emissions of NO<sub>x</sub> and NH<sub>3</sub> are  
217 from the GFED-v2 inventory (van der Werf et al., 2006). Natural NH<sub>3</sub> emissions  
218 include both terrestrial and ocean emissions from the GEIA inventory (Bouwman et  
219 al., 1997).

220

221 The REAS-v2 emission inventory is estimated based on activity data and emission  
222 factors separated by different source categories (Kurokawa et al., 2013). Major NO<sub>x</sub>  
223 sources include fuel combustion in power plants, industry, transport and domestic  
224 sectors, and NH<sub>3</sub> sources are mainly from fertilizer use and manure management of  
225 livestock and human waste (Kurokawa et al., 2013). The sectorial information allows  
226 us to quantify nitrogen deposition contributions from different source categories in the  
227 adjoint analysis as discussed in Section 5.

228

229 The REAS-v2 NH<sub>3</sub> inventory consists of constant annual emissions without any  
230 seasonal variation (Kurokawa et al., 2013). Here we keep the annual total NH<sub>3</sub>  
231 emissions from REAS-v2 and derive monthly scalars over each model grid cell for  
232 NH<sub>3</sub> from different sectors (fertilizer use, livestock and human waste). NH<sub>3</sub> emissions  
233 from fertilizer use are controlled by soil properties, meteorology, and the timing of  
234 fertilizer application. We follow the method and formula given in Skjøth et al. (2011)  
235 and Paulot et al. (2014). We consider nine types of crops (early rice/late rice, winter  
236 wheat/spring wheat, maize, cotton, sweet potatoes, potatoes, fruit and vegetables)  
237 with the harvest areas given by Monfreda et al. (2008). The growth cycles of those  
238 crops and their fertilizer inputs at different application time are based on Liao et al.  
239 (1993) and Sacks et al. (2010). For NH<sub>3</sub> emissions from livestock and human waste,  
240 we use the temperature-dependent experimental formula from Aneja et al. (2000). For

241 the diurnal variability, the NH<sub>3</sub> agricultural emissions are increased by 90% during  
242 the day and reduced by 90% at night following Zhu et al. (2013). Here we have not  
243 considered air-surface bi-directional exchange of NH<sub>3</sub> (Sutton et al., 1998), and treat  
244 the NH<sub>3</sub> fluxes as uncoupled emission and deposition processes.

245

246 Figure 1 shows the spatial distribution of annual total NH<sub>3</sub> and NO<sub>x</sub> emissions over  
247 Asia. Monthly NH<sub>3</sub> and NO<sub>x</sub> emissions from different source types over this region  
248 are also shown in Fig. 1 and the annual totals for Asia and China are summarized in  
249 Table 2. The largest NH<sub>3</sub> emissions are over the eastern China and India with values  
250 over 50 kg N ha<sup>-1</sup> a<sup>-1</sup>. We estimate strong seasonality for the NH<sub>3</sub> emissions from  
251 fertilizer use mainly determined by its usage timing, and from livestock and human  
252 waste depending on surface temperature. Asian NH<sub>3</sub> emissions are highest in  
253 May-August, and a factor of 3 higher than emissions in winter, similar to the  
254 seasonality of US NH<sub>3</sub> emissions in Zhang et al. (2012) derived by NH<sub>x</sub> (NH<sub>3</sub> gas +  
255 aerosol NH<sub>4</sub><sup>+</sup>) surface concentration measurements and in Zhu et al. (2013)  
256 constrained by TES NH<sub>3</sub> observations. Natural NH<sub>3</sub> emissions account for 5% of the  
257 total Asian NH<sub>3</sub> emissions in summer, 11% in winter, and 7% annually. 24% of the  
258 natural NH<sub>3</sub> emissions are from the oceanic emissions (0.50 Tg N a<sup>-1</sup>) over the region.  
259 Recent studies suggested that the GEIA NH<sub>3</sub> oceanic emissions were too high (Paulot  
260 et al., 2015). Anthropogenic NO<sub>x</sub> emissions show weak seasonal variation, consistent  
261 with other emission estimates (Streets et al., 2003; Zhang et al., 2009). Natural NO<sub>x</sub>  
262 emissions (lightning, soil, and biomass burning) account for 23% of the total Asian  
263 NO<sub>x</sub> emissions in summer, 8% in winter, and 16% annually.

264

265 Annual NH<sub>3</sub> and NO<sub>x</sub> emissions over China are respectively 12.8 and 7.9 Tg N a<sup>-1</sup>  
266 (REAS-v2 anthropogenic and natural emissions). Our NH<sub>3</sub> emissions are at the high  
267 end of the range of 7.9-13.2 Tg N a<sup>-1</sup> in the published Chinese NH<sub>3</sub> emission estimates  
268 (Streets et al., 2003; Dong et al., 2010; Paulot et al., 2014 (and references therein)).  
269 This is mainly attributed to a higher estimate of NH<sub>3</sub> from fertilizer use in REAS-v2  
270 (7.8 Tg N a<sup>-1</sup>) than other emission inventories (e.g., 3.2 Tg N a<sup>-1</sup> in Huang et al.

271 (2012)). The successful simulation of NH<sub>3</sub> column concentrations and ammonium wet  
 272 deposition fluxes as described below lends support to the high Chinese NH<sub>3</sub> emissions.  
 273 Comparing with nitrogen emissions in the US (2.9 Tg N a<sup>-1</sup> as NH<sub>3</sub>, and 6.3 Tg N a<sup>-1</sup>  
 274 as NO<sub>x</sub>) (Zhang et al., 2012), NH<sub>3</sub> emissions in China are a factor of 4 higher,  
 275 reflecting its high levels of agricultural activities as well as the population.

276

### 277 2.3 The adjoint model

278

279 The adjoint method provides an efficient way to calculate the sensitivity of model  
 280 variables (e.g., concentrations and deposition fluxes) to model parameters (e.g.,  
 281 emissions). Here we briefly describe the adjoint method, and more details are given in  
 282 Henze et al. (2007). Mathematically, the GEOS-Chem model can be viewed as a  
 283 numerical operator  $\mathbf{F}$ :  $\mathbf{y}_{n+1} = \mathbf{F}(\mathbf{y}_n, \mathbf{x})$ , where  $\mathbf{y}_n$  is the vector of concentrations at  
 284 time step  $n$ , and  $\mathbf{x}$  is the vector of model parameters such as emissions. If we define a  
 285 model response function,  $\mathbf{J}$  (e.g., model deposition), and let  $\lambda_{\mathbf{x}}^n = \left(\frac{\partial \mathbf{J}}{\partial \mathbf{x}_n}\right)^T$  and  
 286  $\lambda_{\mathbf{y}}^n = \left(\frac{\partial \mathbf{J}}{\partial \mathbf{y}_n}\right)^T$ , then  $\lambda_{\mathbf{x}}^0 = \nabla_{\mathbf{x}} \mathbf{J}$  represents the sensitivity of  $\mathbf{J}$  to model parameters, and  
 287  $\lambda_{\mathbf{y}}^0 = \nabla_{\mathbf{y}_0} \mathbf{J}$  represents its sensitivity to the initial conditions. In the adjoint model they  
 288 are computed simultaneously backwards:

$$289 \quad \lambda_{\mathbf{y}}^{n-1} = \left(\frac{\partial \mathbf{F}}{\partial \mathbf{y}}(\mathbf{y}_{n-1}, \mathbf{x})\right)^T \lambda_{\mathbf{y}}^n \quad (1)$$

$$290 \quad \lambda_{\mathbf{x}}^{n-1} = \left(\frac{\partial \mathbf{F}}{\partial \mathbf{x}}(\mathbf{y}_{n-1}, \mathbf{x})\right)^T \lambda_{\mathbf{y}}^n + \lambda_{\mathbf{x}}^n \quad (2)$$

291 where  $\left(\frac{\partial \mathbf{F}}{\partial \mathbf{y}}(\mathbf{y}_{n-1}, \mathbf{x})\right)^T$  and  $\left(\frac{\partial \mathbf{F}}{\partial \mathbf{x}}(\mathbf{y}_{n-1}, \mathbf{x})\right)^T$  are the transpose of the model Jacobian  
 292 matrix.

293

294 The adjoint of GEOS-Chem was constructed by Henze et al (2007) for constraining  
 295 aerosol sources, and extended by Kopacz et al., (2009) for inverse estimates of CO  
 296 sources. The GEOS-Chem adjoint explicitly includes transport components

lin zhang 15/9/1 12:09 PM

已删除: model adjoint operators representing

298 (advection, boundary layer mixing, and convection), gas-phase chemistry, and  
299 heterogeneous chemistry (Henze et al., 2007; 2009). The adjoint of the ISORROPIA  
300 aerosol thermodynamic equilibrium model was constructed by Capps et al. (2012).

301

302 The GEOS-Chem adjoint model has been evaluated and applied in a number of  
303 studies, including optimizing aerosol emission (Henze et al., 2009; Zhu et al., 2013),  
304 attributing sources of ozone pollution in the western US (Zhang et al., 2009), and  
305 quantifying processes affecting nitrogen deposition to biodiversity hotspots worldwide  
306 (Paulot et al., 2013; 2014). Those studies used the adjoint model at global  $4^\circ \times 5^\circ$  or  
307  $2^\circ \times 2.5^\circ$  resolution. The adjoint of the nested-grid GEOS-Chem has been developed  
308 by Jiang et al. (2015) and Zhang et al. (2015), and applied to constrain black carbon  
309 emissions (Mao et al., 2014) and assess human exposure to Equatorial Asian fires  
310 (Kim et al., 2015). Here we apply it to quantify sources contributing to atmospheric  
311 nitrogen deposition over the northwestern Pacific.

312

### 313 **3 Column concentrations and wet deposition fluxes over Asia**

314

315 We compare model simulation of  $\text{NH}_3$  tropospheric columns with satellite  
316 measurements from the Tropospheric Emissions Spectrometer (TES) (Beer 2006), and  
317  $\text{NO}_2$  tropospheric columns with those from the Ozone Monitoring Instrument (OMI)  
318 (Levelt et al., 2006). Both are aboard the NASA Aura satellite in a sun-synchronous  
319 orbit with an ascending equator crossing time of 13:45 (Beer 2006). We evaluate  
320 model simulated wet deposition fluxes of ammonium and nitrate with observational  
321 data from the Acid Deposition Monitoring Network in East Asia (EANET; data  
322 available at <http://www.eanet.asia/index.html>) and ten sites monitored by the Chinese  
323 Academy of Science (CAS) located in North China (Pan et al., 2012). Measurements  
324 of nitrogen dry deposition fluxes are rather limited over the northwestern Pacific.

325

326 Figure 2 compares GEOS-Chem simulated  $\text{NH}_3$  and  $\text{NO}_2$  tropospheric columns with  
327 satellite measurements. These comparisons provide valuable tests of the nitrogen

lin zhang 15/9/1 11:38 AM

已删除: These comparisons provide valuable tests of the nitrogen emissions in the model.

330 emissions and their spatial distributions in the model since both NH<sub>3</sub> and NO<sub>2</sub> have  
331 short lifetimes in the atmosphere. Although NO<sub>2</sub> has a small dry deposition velocity  
332 (Table 1), it rapidly converts to other NO<sub>y</sub> species, thus NO<sub>2</sub> emissions still largely  
333 control the deposition of NO<sub>y</sub>.  
334  
335 The top panels of Figure 2 compare TES measured and GEOS-Chem simulated NH<sub>3</sub>  
336 tropospheric columns in summer (June-August). TES is an infrared Fourier transform  
337 spectrometer with high spectral resolution of 0.06 cm<sup>-1</sup> (Beer, 2006). The  
338 observations have a spatial resolution of 5×8 km<sup>2</sup> with global coverage achieved in 16  
339 days. NH<sub>3</sub> retrievals from TES are based on the optimal estimation method of  
340 Rodgers (2000), as described by Shephard et al. (2011). Following Zhu et al. (2013)  
341 that used TES NH<sub>3</sub> observations to optimize the US NH<sub>3</sub> emissions, we filter the TES  
342 observations based on the retrieval quality control flags, and only use the daytime  
343 observations with cloud optical depth < 1.0. We use TES observations in summer as  
344 they generally have the highest sensitivities during the year (Shephard et al., 2011),  
345 and use observations collected from 2005 to 2010 to increase the number of  
346 observations for comparison. The GEOS-Chem model results for 2009 are sampled  
347 along the TES orbit tracks at the overpass time (The standard TES products are  
348 Level-2 data due to the sparse daily spatial coverage), and then applied with the TES  
349 retrieval operator following Zhang et al. (2006) and Zhu et al. (2013). As shown in  
350 Figure 2, the model generally captures the observed high NH<sub>3</sub> columns over the North  
351 and Northeast China, and India (correlation coefficient  $r = 0.53$ ). The model largely  
352 underestimates NH<sub>3</sub> columns over India by 28%, which suggests NH<sub>3</sub> emissions over  
353 India are too low. For observations over China, the model only has a small negative  
354 bias of 3%.

355  
356 The bottom panels of Figure 2 compare OMI measured and GEOS-Chem simulated  
357 NO<sub>2</sub> tropospheric columns averaged over March-November 2009. OMI measures  
358 backscattered solar radiation over the 270–500 nm wavelength range, and has a  
359 spatial resolution of 13×24 km<sup>2</sup> and daily global coverage (Levelt et al., 2006). We

lin zhang 15/9/1 11:38 AM

已删除: s

lin zhang 15/9/1 11:38 AM

已删除: also

lin zhang 15/9/1 11:39 AM

已删除: s

lin zhang 15/9/1 11:56 AM

已删除: ; Boersma et al., 2011

364 use the [DOMINO v2.0 NO<sub>2</sub> data](#) from KNMI (Boersma et al., 2011;  
365 <http://www.temis.nl/>). [To facilitate the comparison we use the monthly gridded](#)  
366 [tropospheric NO<sub>2</sub> column data which are averages of the retrievals with cloud](#)  
367 [radiance fraction < 50% \(\[http://www.temis.nl/docs/readme\\\_tomsascii.pdf\]\(http://www.temis.nl/docs/readme\_tomsascii.pdf\)\).](#) The  
368 [DOMINO NO<sub>2</sub> data has been validated against surface and aircraft observations](#)  
369 [\(Boersma et al., 2008; 2009; Hains et al., 2010\), and used to constrain NO<sub>x</sub> emissions](#)  
370 [in the model \(Boersma et al., 2008; Lamsal et al., 2010\).](#) The wintertime  
371 measurements are excluded due to large retrieval errors over snow (O'Byrne et al.,  
372 2010). The model generally captures the observed distribution of NO<sub>2</sub> tropospheric  
373 columns over Asia ( $r = 0.93$ ), but it is biased low by 15% over North China on  
374 average. [Recent studies have indicated that DOMINO NO<sub>2</sub> columns might be biased](#)  
375 [high due to the a priori profile shape, error in the surface air-mass factor, and](#)  
376 [exclusion of aerosols in the retrieval \(Hains et al., 2010; Lamsal et al., 2010; Lin et al.,](#)  
377 [2014\).](#) The comparison also did not apply the averaging kernels to the model  
378 [simulated columns, which may lead to additional biases when simulated NO<sub>2</sub> vertical](#)  
379 [profiles are different from the a priori profiles used in the OMI retrievals \(Huijnen et](#)  
380 [al., 2010\),](#)

381  
382 We compare in Figure 3 the observed vs. simulated seasonal mean ammonium and  
383 nitrate wet deposition fluxes at the EANET and CAS monitoring sites. The EANET  
384 data and model results are averaged for January 2008-December 2010, and the CAS  
385 data are for December 2007-November 2010. We compute the correlation coefficient  
386 and the normalized mean bias ( $NMB = \sum_{i=1}^N (M_i - O_i) / \sum_{i=1}^N O_i$ ) between the  
387 observations (O) and model results (M) for the  $N$  monitoring sites. The model  
388 simulation is in good agreement with the observations for both ammonium and nitrate  
389 wet deposition fluxes. For all seasons the correlation coefficients are [greater](#) than 0.7  
390 and NMB values are less than 15%. Annually model simulated nitrogen wet  
391 deposition ( $NH_4^+ + NO_3^-$ ) fluxes over China averages  $9.3 \text{ kg N ha}^{-1} \text{ a}^{-1}$  with  $NH_4^+$   
392 contributing 70%. [Compared with previous studies using ensembles of surface](#)  
393 [measurements, our estimated annual nitrogen wet deposition over China is ~30%](#)

lin zhang 15/9/1 11:56 AM

已删除: monthly OMI

lin zhang 15/9/1 11:56 AM

已删除: (DOMINO v2.0)

lin zhang 15/9/1 11:39 AM

已删除: A recent study by Lin et al. (2014) suggested that DOMINO NO<sub>2</sub> columns might be biased high due to overestimates of surface pressure and exclusion of aerosols in the retrieval.

lin zhang 15/9/1 11:18 AM

已删除: great

402 lower than the estimates of 13.9 kg N ha<sup>-1</sup> a<sup>-1</sup> by Jia et al. (2014) and 13.2 kg N ha<sup>-1</sup>  
403 a<sup>-1</sup> by Zhu et al. (2015a), but is consistent with 9.88 kg N ha<sup>-1</sup> a<sup>-1</sup> by Lv and Tian  
404 (2007). The NH<sub>4</sub><sup>+</sup> contribution to wet deposition is higher than that estimated by Zhu  
405 et al. (2015a) (55%), but is consistent with Lv and Tian (2007) (72%) and Pan et al.  
406 (2012) (63-78% over North China).

407

408 Previous studies have shown that model simulation of wet deposition flux is highly  
409 sensitive to the model precipitation (Pinder et al., 2006; Paulot et al., 2014). We  
410 evaluate the GEOS-5 precipitation data over the northwestern Pacific with data from  
411 the CPC Merged Analysis of Precipitation (CMAP). The CMAP data are based on  
412 several satellite measurements as described in Xie and Arkin (1997), and have a  
413 spatial resolution of 2.5° × 2.5° and monthly variation (data available at  
414 [http://www.cpc.ncep.noaa.gov/products/global\\_precip/html/wpage.cmap.html](http://www.cpc.ncep.noaa.gov/products/global_precip/html/wpage.cmap.html)).

415 Figure 4 compares the monthly averaged GEOS-5 precipitation data with CMAP in  
416 January, April, July and October 2009. Both CMAP and GEOS-5 show maximum  
417 precipitation over the northwestern Pacific Ocean in July and minimum in January.  
418 The GEOS-5 precipitation data generally agree well with the CMAP data ( $r =$   
419 0.83-0.92), with only small negative biases of 2-5% over the ocean.

420

421 To focus on the northwestern Pacific, we further examine the measured and simulated  
422 nitrogen wet deposition fluxes at nine coastal EANET sites. Figure 5 shows locations  
423 of these monitoring sites and the focused region of this study. Figure 6a and 6b  
424 compare the observed vs. simulated monthly mean ammonium and nitrate wet  
425 deposition fluxes at the nine coastal sites. For the sites over the continent, both  
426 ammonium and nitrate wet deposition fluxes show summer maximum and winter  
427 minimum, consistent with seasonal variation of nitrogen emissions and precipitation.  
428 For the island sites in the open ocean (Cheju and Hedo), the deposition fluxes are  
429 much smaller with much weaker seasonal variations. Overall the model closely  
430 reproduces the magnitudes and variability of the measured wet deposition fluxes.

431

lin zhang 15/9/1 11:13 AM

已删除: This is similar to Lv et al (2007) that estimated a mean nitrogen wet deposition flux of 9.88 kg N ha<sup>-1</sup> a<sup>-1</sup> over China with 72% from NH<sub>4</sub><sup>+</sup> wet deposition using an ensemble of precipitation chemistry data.

## 437 4 Nitrogen deposition to the northwestern Pacific

### 438 4.1 Seasonal variation and deposition process

439

440 We now examine the deposition processes, patterns, and seasonal variation of  
441 atmospheric nitrogen deposition to the northwestern Pacific. Figure 7 shows the  
442 spatial distribution of total nitrogen deposition (ammonium and nitrate, dry and wet)  
443 to the northwestern Pacific in January, April, July and October, and Figure 8 shows  
444 annual total deposition fluxes average over 2008-2010. Unlike the strong seasonality  
445 in nitrogen deposition over the Asian continent, deposition over the ocean has weaker  
446 seasonality as also shown by the wet deposition fluxes in Figure 6. At low latitudes  
447 ( $<30^{\circ}\text{N}$ ) or over the oceans east of Japan, we can see nitrogen deposition reaches its  
448 maximum in January and is lowest in July. At middle latitudes ( $>30^{\circ}\text{N}$ ) along the  
449 eastern China coast, nitrogen deposition peaks in July with the highest values greater  
450 than  $2 \text{ kg N ha}^{-1} \text{ month}^{-1}$  along the coastlines. In all seasons, deposition decreases  
451 rapidly downwind of the continental sources. Jung et al. (2011) using aerosol and rain  
452 samples estimated total nitrogen deposition fluxes of  $32\text{-}64 \mu\text{mol m}^{-2} \text{ d}^{-1}$  ( $1.6\text{-}3.3 \text{ kg N}$   
453  $\text{ha}^{-1} \text{ a}^{-1}$ ) in the central Pacific Ocean with 66-99% via wet deposition. Our model  
454 shows similar results ( $0.8\text{-}4 \text{ kg N ha}^{-1} \text{ a}^{-1}$ ).

455

456 We selected two regions as shown in Figure 7 representing the Yellow Sea and the  
457 South China Sea. Table 3 summarizes the monthly and annual nitrogen deposition  
458 fluxes over the two regions for 2008-2010. Nitrogen deposition averages  $11.9 \text{ kg N}$   
459  $\text{ha}^{-1} \text{ a}^{-1}$  over the Yellow Sea ( $5.0 \text{ kg N ha}^{-1} \text{ a}^{-1}$  as reduced nitrogen  $\text{NH}_x$  and  $6.9 \text{ kg N}$   
460  $\text{ha}^{-1} \text{ a}^{-1}$  as oxidized nitrogen  $\text{NO}_y$ ). Seasonal variation of the deposition to the Yellow  
461 Sea is weak with fluxes in October and January about 10% higher than in April and  
462 July. Nitrogen deposition to the South China Sea averages  $5.6 \text{ kg N ha}^{-1} \text{ a}^{-1}$  with  
463 deposition in January nearly a factor of 3 higher than deposition in July. This reflects  
464 seasonal variations in both meteorology and nitrogen emissions as will be discussed  
465 below.

466



467 Wet deposition accounts for 67% of the total nitrogen deposition to the Yellow Sea  
468 (82% for  $\text{NH}_x$  and 57% for  $\text{NO}_y$ ) and the South China Sea (84% for  $\text{NH}_x$  and 55% for  
469  $\text{NO}_y$ ). The ratio of wet vs. dry deposition over the ocean is generally higher than that  
470 over the land, because of slow dry deposition velocities (Table 1) and less nitrogen  
471 exported near the surface, particularly for reduced nitrogen. Simulated nitrogen  
472 deposition fluxes are in the range of 20-55  $\text{kg N ha}^{-1} \text{ a}^{-1}$  in the eastern China, with wet  
473 deposition accounting for 65% of the  $\text{NH}_x$  deposition and 54% of the  $\text{NO}_y$  deposition  
474 (Figure not shown).

475

#### 476 **4.2 Contribution from the oceanic emissions**

477

478 It is important to separate the contributions of ocean vs. land emissions to the nitrogen  
479 deposition over the northwestern Pacific. Sources of fixed nitrogen from the ocean  
480 include both anthropogenic ship  $\text{NO}_x$  emissions and natural oceanic  $\text{NH}_3$  emissions.  
481 Those emissions are small compared with land sources, but their contributions to the  
482 nitrogen deposition over the open ocean cannot be neglected due to the short lifetimes  
483 of nitrogen species. We have conducted two sensitivity simulations respectively with  
484 ship  $\text{NO}_x$  emissions or oceanic  $\text{NH}_3$  emissions shut off. The differences with the  
485 standard simulation represent contributions of each source to the nitrogen deposition.

486

487 We separate in Figure 8 the annual contributions of nitrogen sources over land, ship  
488  $\text{NO}_x$  emissions, and oceanic  $\text{NH}_3$  emissions to total nitrogen deposition over the  
489 northwestern Pacific. We can see nitrogen deposition to the marginal seas of the  
490 northwestern Pacific is dominated by transport of nitrogen sources over the Asian  
491 continent. Ship  $\text{NO}_x$  and oceanic  $\text{NH}_3$  emissions contribute little nitrogen deposition  
492 (together less than 1%) to the Yellow Sea, and about 7% over the South China Sea.  
493 Further to the equatorial Pacific Ocean ship  $\text{NO}_x$  emissions contribute 10-25% of the  
494 total nitrogen deposition along the ship tracks. And oceanic  $\text{NH}_3$  emissions account  
495 for 15-40% of the total nitrogen deposition annually.

496

### 497 4.3 Outflow from Mainland China

498

499 We have demonstrated above that nitrogen deposition to the marginal seas of the  
500 northwestern Pacific such as the Yellow Sea and the South China Sea mainly  
501 originates from nitrogen sources over the land. We now focus on the outflow fluxes  
502 from Mainland China where the largest nitrogen emissions are located. Figure 9  
503 shows the outflow fluxes of fixed nitrogen transported across the coastline of  
504 Mainland China (as defined by the grid cells in Figure 5) in different seasons. Fluxes  
505 of  $\text{NH}_3$ ,  $\text{NH}_4^+$ ,  $\text{HNO}_3$ , isoprene nitrates, and  $\text{NO}_3^-$  are included. Other fixed nitrogen  
506 species such as PAN, although important in outflow fluxes, account for less than 1%  
507 of the nitrogen deposition to the northwestern Pacific.

508

509 We can see that the spatial and seasonal variations of atmospheric nitrogen deposition  
510 over the marginal seas of the northwestern Pacific as shown in Figure 7 can be mainly  
511 explained by variations of outflow fluxes from China. Nitrogen outflow fluxes across  
512 the eastern coastline (cell 1-14 in Figure 5) to the Yellow Sea show strong transport  
513 from Jiangsu Province (cell 7-14 in Figure 5) below 800 hPa corresponding to the  
514 maximum nitrogen deposition near the east coast of China in July. Fluxes in April and  
515 October are strong in the free troposphere, where the lifetimes of nitrogen species are  
516 longer than in the boundary layer leading to deposition further to the open ocean of  
517 the Yellow Sea. Over the southern coastline (cell 20-38 in Figure 5) to the South  
518 China Sea, nitrogen fluxes are largest within the boundary layer in January and  
519 October. The fluxes turn to inflow in April and July, minimizing deposition to the  
520 South China Sea during these months.

521

522 The seasonal variation of pollution transport over the eastern Asia is largely  
523 controlled by the East Asian monsoon system (Liu et al., 2003; Liang et al., 2004;  
524 Zhang et al., 2010). We show in Figure 10 the monthly mean wind fields averaged in  
525 the boundary layer (generally below 950 hPa) and in the free troposphere at 700 hPa  
526 plotted over the monthly emissions of fixed nitrogen. In January the northwesterly

527 monsoon prevails at middle latitudes ( $> 30^\circ$ ) in the boundary layer and gradually turns  
528 to the northeasterly at lower latitudes ( $< 30^\circ$ ). Asian pollution is generally trapped in  
529 the boundary layer by the large-scale subsidence over the continent and transported  
530 southward as shown in Figure 9. In July, the summer southerly monsoon winds bring  
531 clean ocean air to the southern China, but at latitudes north of  $30^\circ\text{N}$  the southwesterly  
532 winds combined with the high nitrogen emissions over the eastern China lead to large  
533 fluxes to the Yellow Sea. Spring and fall represent the transitional periods, and  
534 frequent cold fronts are the primary driver lifting anthropogenic pollution to the free  
535 troposphere followed by westerly transport (Liu et al., 2003; Liang et al., 2004).

536

537 Thus the strong seasonal variation in nitrogen deposition to the South China Sea is  
538 mainly attributed to the monsoonal Asian outflow. Over the Yellow Sea, we find the  
539 weaker winds in July can be compensated by higher nitrogen emissions over the land,  
540 leading to the weak seasonality of nitrogen deposition. We find in a sensitivity  
541 simulation without seasonal variations of Asian  $\text{NH}_3$  emissions that nitrogen  
542 deposition to the Yellow Sea would have been 64% higher in January than July.

543

#### 544 **5 Source attribution using the adjoint method**

545

546 The adjoint model allows us to further quantify the sources contributing to  
547 atmospheric nitrogen deposition over the receptors at the model underlying grid scale.  
548 Here we calculate the sensitivities of nitrogen deposition (reduced and oxidized  
549 nitrogen, wet and dry) over the Yellow Sea and the South China Sea to grid-resolved  
550  $\text{NH}_3$  and  $\text{NO}_x$  emissions for January, April, July and October 2009. For each month,  
551 we calculate sensitivity of the monthly mean nitrogen deposition to emissions in that  
552 month and a week in the preceding month (accounting for the lifetimes of nitrogen  
553 species). We separate the sensitivities to different source types (e.g., fertilizer and  
554 livestock for  $\text{NH}_3$ , and industry and power plants for  $\text{NO}_x$ ) based on their relative  
555 contributions to the total anthropogenic emissions.

556

557 The top panels of Figure 11 show the adjoint sensitivities for the monthly total  
558 nitrogen deposition to the Yellow Sea. The magnitude of adjoint sensitivity reflects  
559 deposition amount contributed by the nitrogen emissions in each grid cell. The sum of  
560 sensitivities integrated geographically matches the monthly deposition flux to the  
561 Yellow Sea within 5%. From winter to summer the source regions move southward  
562 from North China and Northeast China to East China and Central China, consistent  
563 with the seasonal variation of the monsoonal flow. Nitrogen sources over China are  
564 the main contributor to the nitrogen deposition to the Yellow Sea (93% in January, 88%  
565 in July, and 92% annually). Sources over the Korean peninsula contribute 7% of  
566 annual nitrogen deposition to the Yellow Sea.

567

568 The bottom panels of Figure 11 separate the sensitivities of nitrogen deposition  
569 components (reduced and oxidized nitrogen, wet and dry) to emissions from different  
570 source types. The total sensitivity of each deposition component also approximately  
571 matches the simulated deposition flux (Table 3), with small discrepancies of 0.01-0.06  
572  $\text{kg N ha}^{-1} \text{ month}^{-1}$  that can be attributed to nonlinearity between nitrogen deposition  
573 and emissions (including nitrogen,  $\text{SO}_2$ , and VOC emissions) as discussed in Paulot et  
574 al. (2013). Figure 11 shows that  $\text{NO}_x$  emissions from power plants (37%), followed by  
575 emissions from transport (26%) and industry (22%) contribute most of the nitrogen  
576 deposition in January. In other months,  $\text{NH}_3$  emissions from fertilizer use (25-32%)  
577 are the largest source of nitrogen deposition to the Yellow Sea. Annually the major  
578 sources contributing to nitrogen deposition to the Yellow Sea are fertilizer use (24%),  
579 power plants (22%), and transportation (18%).

580

581 Figure 12 shows source attribution of atmospheric nitrogen deposition to the South  
582 China Sea. Unlike that to the Yellow Sea, nitrogen deposition to the South China Sea  
583 shows a distinct winter peak as reflected by the largest source contributing areas in  
584 January spreading over the Asian continent. Kim et al. (2014) using back trajectories  
585 suggested transport of nitrogen from the east coasts of China and Indonesia to the  
586 South China Sea. Here we estimate that nitrogen deposition to the South China Sea is

587 mainly from Mainland China and Taiwan, contributing 66% and 20% of the annual  
588 total nitrogen deposition. The rest 14% results from sources over the Southeast Asian  
589 countries as well as oceanic  $\text{NH}_3$  emissions.

590

591 For the sectorial contributions, nitrogen sources from power plants, transport, industry,  
592 and fertilizer use show comparable contribution to nitrogen deposition over the South  
593 China Sea in January (16-21%) and October (14-23%). But in April and July,  
594 fertilizer use and natural emissions become most significant. In April, natural  
595 emissions account for 17% of the nitrogen deposition to the South China Sea mainly  
596 via wet deposition, including 7% from the oceanic  $\text{NH}_3$  emissions, 4% from lightning,  
597 and 6% from biomass burning emissions over Southeast Asia.

598

599 One interesting feature we can see from Figure 11 and Figure 12 is that anthropogenic  
600  $\text{NO}_y$  dry deposition exhibits different response to increasing  $\text{NH}_3$  emissions over the  
601 Yellow Sea (negative) and the South China Sea (near zero). It indicates that reducing  
602  $\text{NH}_3$  emissions would even enhance dry deposition of  $\text{NO}_y$  to the Yellow Sea. We  
603 show in Figure 13 the sensitivity of  $\text{NO}_y$  dry deposition to  $\text{NH}_3$  emissions for  
604 deposition to the Yellow sea and to the South China Sea in January 2009. The values  
605 are generally negative for the Yellow Sea, and positive for the South China Sea  
606 except for the areas near the coast.

607

608 This can be explained by the conversion of  $\text{HNO}_3$  to aerosol  $\text{NO}_3^-$  and their different  
609 dry deposition velocities. Dry deposition velocities for aerosol nitrate is much slower  
610 than  $\text{HNO}_3$  gas (Table 1).  $\text{NH}_3$  emissions would lead to formation of aerosol  $\text{NO}_3^-$   
611 from  $\text{HNO}_3$ , increasing the lifetime of  $\text{NO}_y$  and allowing them transport to a longer  
612 distance. It would thus decrease the dry deposition of  $\text{NO}_y$  (mainly via reduction of  
613  $\text{HNO}_3$ ) near the source region (e.g., the Yellow Sea), and enhance its dry deposition  
614 further downwind (e.g., the South China Sea). The same response applies to  $\text{NH}_x$  dry  
615 deposition and  $\text{NO}_x$  emissions (the April panel of Figure 11), but it is much weaker  
616 because  $\text{NH}_x$  dry deposition fluxes to the ocean are small and mainly from dry

617 deposition of aerosol  $\text{NH}_4^+$ . This can have important implications on the effectiveness  
618 of the emission control strategy for reducing nitrogen deposition to the Yellow Sea.  
619 As shown in Figure 11,  $\text{NH}_3$  emissions from fertilizer use are identified as the largest  
620 contributor to nitrogen deposition to the Yellow Sea except in winter. However, we  
621 estimate annually 28% (negative sensitivity of  $\text{NO}_y$  dry deposition vs. sensitivity of  
622  $\text{NH}_x$  total deposition to  $\text{NH}_3$  emissions, averaged over the four months in Figure 11)  
623 of the expected benefits of reduction of nitrogen deposition to the Yellow Sea via  
624 controlling  $\text{NH}_3$  would be offset by an increase in  $\text{NO}_y$  dry deposition.

625

## 626 **6 Conclusions**

627

628 Increasing atmospheric nitrogen deposition to the northwestern Pacific has likely been  
629 altering the marine environment. The purpose of this study is to quantify the sources,  
630 processes, and seasonal variation of atmospheric nitrogen deposition to the  
631 northwestern Pacific. We have used a nested-grid version of the GEOS-Chem global  
632 chemistry model and its adjoint model to address the issue. The model has a  
633 horizontal resolution of  $1/2^\circ$  latitude  $\times$   $2/3^\circ$  longitude over the East Asia and its  
634 adjacent oceans ( $70^\circ\text{E}$ - $150^\circ\text{E}$ ,  $11^\circ\text{S}$ - $55^\circ\text{N}$ ), and  $4^\circ \times 5^\circ$  over the rest of the world. It  
635 includes a detailed tropospheric chemistry to simulate the sources, transformation, and  
636 deposition of fixed nitrogen ( $\text{NH}_x$  and  $\text{NO}_y$ ) in the atmosphere.

637

638 The model uses the anthropogenic emissions of fixed nitrogen (via  $\text{NH}_3$  and  $\text{NO}_x$ )  
639 from the REAS-v2 emission inventory for Asia (Kurokawa et al., 2013). The original  
640  $\text{NH}_3$  emissions had no seasonal variation, inconsistent with recent Asian  $\text{NH}_3$   
641 emission estimates. We calculate the seasonal variations for  $\text{NH}_3$  emissions from  
642 fertilizer use based on soil properties, meteorology, and the timing of fertilizer  
643 application (Skj  th et al., 2011; Paulot et al., 2014), and for  $\text{NH}_3$  from livestock and  
644 human waste using surface temperature (Aneja et al., 2000). The resulting Asian  $\text{NH}_3$   
645 emissions are highest in May-August, with emissions in summer a factor of 3 higher  
646 than winter. Total Asian  $\text{NH}_3$  and  $\text{NO}_x$  emissions are 28.6 and 16.2 Tg N a<sup>-1</sup>,

647 respectively. China has the largest nitrogen sources with 12.8 Tg N a<sup>-1</sup> as NH<sub>3</sub> and 7.9  
648 Tg N a<sup>-1</sup> as NO<sub>x</sub>. Both NH<sub>3</sub> and NO<sub>x</sub> emissions are dominated by anthropogenic  
649 sources. Natural sources account for 7% for NH<sub>3</sub>, and 16% for NO<sub>x</sub>.

650

651 We evaluate the model simulation of NH<sub>3</sub> and NO<sub>2</sub> tropospheric columns with  
652 satellite observations from TES and OMI over Asia. The model generally captures the  
653 observed distribution of NH<sub>3</sub> and NO<sub>2</sub> tropospheric columns with only small negative  
654 biases for both species (-3% for NH<sub>3</sub> over China and up to -15% for NO<sub>2</sub> over the  
655 North China), providing support to the model emissions. The model further closely  
656 reproduces the magnitudes and variability of ammonium and nitrate wet deposition  
657 fluxes at the EANET sites and additional monitoring sites over the North China. Wet  
658 deposition fluxes measured over the continental sites show strong seasonality with  
659 summer maximum and winter minimum, while for the island sites in the open ocean,  
660 deposition fluxes are much smaller with weak seasonal variations.

661

662 We analyze three-year (2008-2010) model simulation of atmospheric nitrogen  
663 deposition to the northwestern Pacific, particularly over the marginal seas such as the  
664 Yellow Sea and the South China Sea. Atmospheric nitrogen deposition reaches as  
665 high as 20-55 kg N ha<sup>-1</sup> a<sup>-1</sup> in the eastern China, and decreases rapidly downwind of  
666 the Asian continent (0.8-20 kg N ha<sup>-1</sup> a<sup>-1</sup> over the northwestern Pacific). Nitrogen  
667 deposition averages 11.9 kg N ha<sup>-1</sup> a<sup>-1</sup> over the Yellow Sea (5.0 kg N ha<sup>-1</sup> a<sup>-1</sup> as NH<sub>x</sub>  
668 and 6.9 kg N ha<sup>-1</sup> a<sup>-1</sup> as NO<sub>y</sub>), and 5.6 kg N ha<sup>-1</sup> a<sup>-1</sup> to the South China Sea (2.5 as NH<sub>x</sub>  
669 and 3.1 as NO<sub>y</sub>). Although Asian NH<sub>3</sub> emissions are much higher than NO<sub>x</sub> emissions,  
670 less NH<sub>x</sub> is exported and deposited over the open ocean due to its shorter lifetime. We  
671 find contributions of nitrogen sources over the ocean, including ship NO<sub>x</sub> emissions  
672 and oceanic NH<sub>3</sub> emissions, are negligible for nitrogen deposition to the Yellow Sea,  
673 and about 7% over the South China Sea. Further downwind in the ocean ship NO<sub>x</sub>  
674 emissions contribute 10-25% of total nitrogen deposition along the ship tracks, and  
675 oceanic NH<sub>3</sub> emissions are responsible for 15-40% of the nitrogen deposition.

676

677 Seasonal variations in nitrogen deposition to the northwestern Pacific are generally  
678 determined by variations in meteorology and nitrogen emissions. Nitrogen deposition  
679 to the South China Sea showed strong seasonal variation, with deposition in January  
680 ( $0.62 \text{ kg N ha}^{-1} \text{ month}^{-1}$ ) nearly a factor of 3 higher than deposition in July ( $0.23 \text{ kg N}$   
681  $\text{ha}^{-1} \text{ month}^{-1}$ ). This is consistent with the nitrogen outflow fluxes from Asia (mainly  
682 Mainland China), which are controlled by the East Asian monsoon system as  
683 discussed in previous studies (Liu et al., 2003; Zhang et al., 2010). In winter the  
684 northerly monsoon favors transport of Asian pollution to the open ocean in the  
685 boundary layer, while the summer southerly monsoon winds bring clean ocean air to  
686 the southern China. Nitrogen deposition to the Yellow Sea has weak seasonality  
687 ( $0.85\text{-}1.12 \text{ kg N ha}^{-1} \text{ month}^{-1}$ ). We find the weaker winds in summer over the Yellow  
688 Sea suppress dry deposition of nitrogen, but are compensated by higher nitrogen  
689 emissions in summer.

690

691 We have further applied the adjoint of GEOS-Chem to estimate the contributions of  
692 nitrogen sources from different sectors and at the model underlying resolution to  
693 nitrogen deposition over the Yellow Sea and the South China Sea. This detailed  
694 source information can be crucial to design an effective strategy for reducing nitrogen  
695 deposition to these areas. Nitrogen deposition to the Yellow Sea mainly originates  
696 from nitrogen sources over China (92% contribution) and the Korean peninsula (7%)  
697 categorized by regions, and is contributed from fertilizer use (24%), power plants  
698 (22%), and transportation (18%) categorized by emission sectors. For deposition to  
699 the South China Sea, nitrogen sources over Mainland China and Taiwan contribute 66%  
700 and 20% of the annual total deposition, with the rest 14% from sources over the  
701 Southeast Asian countries as well as oceanic  $\text{NH}_3$  emissions. Natural sources are  
702 particularly important in April, accounting for 17% of the nitrogen deposition to the  
703 South China Sea (7% from the oceanic  $\text{NH}_3$  emissions, 4% from lightning, and 6%  
704 from biomass burning emissions over Southeast Asia).

705

706 The adjoint analyses also indicate that dry deposition of oxidized nitrogen to the



707 Yellow Sea shows negative sensitivity to Asian NH<sub>3</sub> emissions, ie., reducing Asian  
708 NH<sub>3</sub> emissions would increase the NO<sub>y</sub> dry deposition to the Yellow Sea. This  
709 response mainly reflects conversion of gaseous NH<sub>3</sub> and HNO<sub>3</sub> to ammonium nitrate  
710 aerosol and their different deposition efficiencies. Annually 28% of the reduction of  
711 nitrogen deposition to the Yellow Sea via reducing NH<sub>3</sub> emissions would be offset by  
712 increases in NO<sub>y</sub> dry deposition, placing a limitation on the effectiveness of NH<sub>3</sub>  
713 emission controls for mitigating nitrogen deposition over the Yellow Sea.

714

715 While this study provides a pilot investigation of the sources and processes  
716 controlling atmospheric nitrogen deposition to the northwestern Pacific, some  
717 uncertainties still need to be considered. A main uncertainty is associated with the  
718 lack of in-situ measurements to evaluate the model simulated nitrogen dry deposition  
719 fluxes. Uncertainties exist in both model calculated dry deposition velocities over the  
720 ocean surface (as discussed in section 2.1) and simulated surface concentrations of  
721 nitrogen species. Recent studies have shown that GEOS-Chem overestimates  
722 wintertime surface concentrations of nitrate and nitric acid (Heald et al., 2012; Zhang  
723 et al., 2012; Wang et al., 2013), which can lead to a model overestimation of NO<sub>y</sub> dry  
724 deposition flux in winter.

725

726 Uncertainties also exist in Asian NH<sub>3</sub> emissions; in particular, air-surface  
727 bi-directional NH<sub>3</sub> fluxes are not considered in the study. Although it has little impact  
728 on the oceanic emissions, recent implementations of the bi-directional NH<sub>3</sub> flux on  
729 fertilizer use showed lower NH<sub>3</sub> agricultural emissions over China (Fu et al., 2015;  
730 Zhu et al., 2015b), and thus would lower its transport to the ocean. In addition, any  
731 bias in the GEOS-Chem simulation would affect the adjoint sensitivity. Also to  
732 ascribe nitrogen deposition to sources from different emission sectors, we rely on the  
733 bottom-up sectorial emissions to separate the adjoint sensitivity. Even though the total  
734 emissions can be constrained with the satellite measurements, the sectorial  
735 information is subject to larger uncertainties (Zhang et al., 2009). We recommend  
736 future research to reduce these uncertainties.

738 **Acknowledgements.** This work was supported by the National Key Basic Research  
739 Program of China (grant 2014CB441303), and by the National Natural Science  
740 Foundation of China (grant 41205103, 41475112, and 41405144). FP and DKH  
741 acknowledge funding support from the NASA Air Quality Applied Science Team  
742 (AQAAT). The authors also acknowledge the work of many individuals who have  
743 made the measurements of EANET, OMI, and TES.

744

## 745 **References**

746 Amos, H. M., Jacob, D. J., Holmes, C. D., Fisher, J. A., Wang, Q., Yantosca, R. M.,  
747 Corbitt, E. S., Galarneau, E., Rutter, A. P., Gustin, M. S., Steffen, A., Schauer, J. J., Graydon,  
748 J. A., St Louis, V. L., Talbot, R. W., Edgerton, E. S., Zhang, Y., and Sunderland, E. M.:  
749 Gas-particle partitioning of atmospheric Hg(II) and its effect on global mercury deposition,  
750 *Atmos. Chem. Phys.*, 12, 591-603, doi:10.5194/acp-12-591-2012, 2012.

751 Aneja, V. P., Chauhan, J. P., and Walker, J. T.: Characterization of atmospheric  
752 ammonia emissions from swine waste storage and treatment lagoons, *J. Geophys.*  
753 *Res.-Atmos.*, 105, 11535-11545, 2000.

754 Beer, R.: TES on the Aura mission: Scientific objectives, measurements, and analysis  
755 overview, *IEEE T. Geosci. Remote*, 44, 1102-1105, 2006.

756 Bey, I., Jacob, D. J., Yantosca, R. M., Logan, J. A., Field, B. D., Fiore, A. M., Li, Q. B.,  
757 Liu, H. G. Y., Mickley, L. J., and Schultz, M. G.: Global modeling of tropospheric chemistry  
758 with assimilated meteorology: Model description and evaluation, *J. Geophys. Res.-Atmos.*,  
759 106, 23073-23095, 2001.

760 Bobbink, R., and Roelofs, J. G. M.: Nitrogen critical loads for natural and semi-natural  
761 ecosystems: The empirical approach, *Water Air Soil. Poll.*, 85, 2413-2418, 1995.

762 [Boersma, K. F., Jacob, D., Bucsel, E., Perring, A., Dirksen, R., van der A, R., Yantosca,](#)  
763 [R., Park, R., Wenig, M., Bertram, T., and Cohen, R.: Validation of OMI tropospheric NO<sub>2</sub>](#)  
764 [observations during INTEX-B and application to constrain NO<sub>x</sub> emissions over the eastern](#)  
765 [United States and Mexico, \*Atmos. Environ.\*, 42\(19\), 4480-4497, 2008.](#)

766 [Boersma, K. F., Jacob, D. J., Trainic, M., Rudich, Y., DeSmedt, I., Dirksen, R., and](#)  
767 [Eskes, H. J.: Validation of urban NO<sub>2</sub> concentrations and their diurnal and seasonal variations](#)  
768 [observed from the SCIAMACHY and OMI sensors using in situ surface measurements in](#)  
769 [Israeli cities, \*Atmos. Chem. Phys.\*, 9, 3867-3879, doi:10.5194/acp-9-3867-2009, 2009.](#)

770 Boersma, K. F., Eskes, H. J., Dirksen, R. J., van der A, R. J., Veefkind, J. P., Stammes,  
771 P., Huijnen, V., Kleipool, Q. L., Sneep, M., Claas, J., Leitao, J., Richter, A., Zhou, Y., and  
772 Brunner, D.: An improved tropospheric NO<sub>2</sub> column retrieval algorithm for the Ozone  
773 Monitoring Instrument, *Atmos. Meas. Tech.*, 4, 1905-1928, doi:10.5194/amt-4-1905-2011,  
774 2011.

775 Bouwman, A. F., Lee, D. S., Asman, W. A. H., Dentener, F. J., VanderHoek, K. W., and  
776 Olivier, J. G. J.: A global high-resolution emission inventory for ammonia, *Global*

777 Biogeochem. Cy., 11, 561-587, 1997.

778 Bouwman, A. F., Van Vuuren, D. P., Derwent, R. G., and Posch, M.: A global analysis  
779 of acidification and eutrophication of terrestrial ecosystems, *Water Air Soil Poll*, 141,  
780 349-382, 2002.

781 Bowman, W. D., Cleveland, C. C., Halada, L., Hresko, J., and Baron, J. S.: Negative  
782 impact of nitrogen deposition on soil buffering capacity, *Nat Geosci*, 1, 767-770, 2008.

783 Capps, S. L., Henze, D. K., Hakami, A., Russell, A. G., and Nenes, A.: ANISORROPIA:  
784 the adjoint of the aerosol thermodynamic model ISORROPIA, *Atmos. Chem. Phys.*, 12,  
785 527-543, doi:10.5194/acp-12-527-2012, 2012.

786 Chen, D., Wang, Y., McElroy, M. B., He, K., Yantosca, R. M., and Le Sager, P.:  
787 Regional CO pollution and export in China simulated by the high-resolution nested-grid  
788 GEOS-Chem model, *Atmos. Chem. Phys.*, 9, 3825-3839, doi:10.5194/acp-9-3825-2009, 2009.

789 Dickerson, R., Li, C., Li, Z., Marufu, L., Stehr, J., McClure, B., Krotkov, N., Chen, H.,  
790 Wang, P., and Xia, X.: Aircraft observations of dust and pollutants over northeast China:  
791 Insight into the meteorological mechanisms of transport, *J. Geophys. Res.-Atmos.*, 112,  
792 D24S90, doi:10.1029/2007JD008999, 2007.

793 Dong, W., Xing, J., and Wang, S. X.: Temporal and spatial distribution of anthropogenic  
794 ammonia emissions in China: 1994-2006, *Environm. Sci.*, 31, 1457-1463, 2010.

795 Duce, R. A., Liss, P. S., Merrill, J. T., Atlas, E. L., Buat-Menard, P., Hicks, B. B., Miller,  
796 J. M., Prospero, J. M., Arimoto, R., Church, T. M., Ellis, W., Galloway, J. N., Hansen, L.,  
797 Jickells, T. D., Knap, A. H., Reinhardt, K. H., Schneider, B., Soudine, A., Tokos, J. J.,  
798 Tsunogai, S., Wollast, R., and Zhou, M.: The atmospheric input of trace species to the world  
799 ocean, *Global Biogeochem. Cy.*, 5, 193-259, 1991.

800 Duce, R. A., LaRoche, J., Altieri, K., Arrigo, K. R., Baker, A. R., Capone, D. G., Cornell,  
801 S., Dentener, F., Galloway, J., Ganeshram, R. S., Geider, R. J., Jickells, T., Kuypers, M. M.,  
802 Langlois, R., Liss, P. S., Liu, S. M., Middelburg, J. J., Moore, C. M., Nickovic, S., Oschlies,  
803 A., Pedersen, T., Prospero, J., Schlitzer, R., Seitzinger, S., Sorensen, L. L., Uematsu, M.,  
804 Ulloa, O., Voss, M., Ward, B., and Zamora, L.: Impacts of atmospheric anthropogenic  
805 nitrogen on the open ocean, *Science*, 320, 893-897, 2008.

806 Evans, M. J., and Jacob, D. J.: Impact of new laboratory studies of N<sub>2</sub>O<sub>5</sub> hydrolysis on  
807 global model budgets of tropospheric nitrogen oxides, ozone, and OH, *Geophys. Res. Lett.*,  
808 32, L09813, doi:10.1029/2005gl022469, 2005.

809 Fountoukis, C., and Nenes, A.: ISORROPIA II: a computationally efficient  
810 thermodynamic equilibrium model for K<sup>+</sup>-Ca<sup>2+</sup>-Mg<sup>2+</sup>-NH<sub>4</sub><sup>+</sup>-Na<sup>+</sup>-SO<sub>4</sub><sup>2-</sup>-NO<sub>3</sub><sup>-</sup>-Cl<sup>-</sup>-H<sub>2</sub>O aerosols,  
811 *Atmos. Chem. Phys.*, 7, 4639-4659, doi:10.5194/acp-7-4639-2007, 2007.

812 [Fu, X., Wang, S. X., Ran, L. M., Pleim, J. E., Cooter, E., Bash, J. O., Benson, V., and](#)  
813 [Hao, J. M.: Estimating NH<sub>3</sub> emissions from agricultural fertilizer application in China using](#)  
814 [the bi-directional CMAQ model coupled to an agro-ecosystem model, \*Atmos. Chem. Phys.\*,](#)  
815 [15, 6637-6649, 10.5194/acp-15-6637-2015, 2015.](#)

816 Galloway, J. N., Dentener, F. J., Capone, D. G., Boyer, E. W., Howarth, R. W.,  
817 Seitzinger, S. P., Asner, G. P., Cleveland, C. C., Green, P. A., Holland, E. A., Karl, D. M.,  
818 Michaels, A. F., Porter, J. H., Townsend, A. R., and Vorosmarty, C. J.: Nitrogen cycles: past,  
819 present, and future, *Biogeochemistry*, 70, 153-226, 2004.

820 [Garfinkel, C. I., Molod, A. M., Oman, L. D., and Song, I. S.: Improvement of the](#)

821 [GEOS-5 AGCM upon updating the air-sea roughness parameterization, \*Geophys. Res. Lett.\*,  
822 38, L18702, doi:10.1029/2011GL048802, 2011.](#)

823 [Hains, J. C., Boersma, K., Kroon, M., Dirksen, R., Cohen, R., Perring, A., Bucsel, E.,  
824 Volten, H., Swart, D., Richter, A., Wittrock, F., Schoenhardt, A., Wagner, T., Ibrahim, O.,  
825 van Roozendaal, M., Pinardi, G., Gleason, J., Veeffkind, P., and Levelt, P.: Testing and  
826 Improving OMI DOMINO Tropospheric NO<sub>2</sub> Using Observations from the DANDELIONS  
827 and INTEXB Validation Campaigns, \*J. Geophys. Res.\*, 115, D05301,  
828 doi:10.1029/2009JD012399, 2010.](#)

829 [Heald, C. L., Collett, J. L., Lee, T., Benedict, K. B., Schwandner, F. M., Li, Y., Clarisse,  
830 L., Hurtmans, D. R., Van Damme, M., Clerbaux, C., Coheur, P. F., Philip, S., Martin, R. V.,  
831 and Pye, H. O. T.: Atmospheric ammonia and particulate inorganic nitrogen over the United  
832 States, \*Atmos. Chem. Phys.\*, 12, 10295-10312, 2012.](#)

833 Henze, D. K., Hakami, A., and Seinfeld, J. H.: Development of the adjoint of  
834 GEOS-Chem, *Atmos. Chem. Phys.*, 7, 2413-2433, doi:10.5194/acp-9-5877-2009, 2007.

835 Henze, D. K., Seinfeld, J. H., and Shindell, D. T.: Inverse modeling and mapping US air  
836 quality influences of inorganic PM<sub>2.5</sub> precursor emissions using the adjoint of GEOS-Chem,  
837 *Atmos. Chem. Phys.*, 9, 5877-5903, doi:10.5194/acp-9-5877-2009, 2009.

838 Hu, C., Li, D., Chen, C., Ge, J., MullerKarger, F. E., Liu, J., Yu, F., and He, M. X.: On  
839 the recurrent *Ulva prolifera* blooms in the Yellow Sea and East China Sea, *J. Geophys. Res.-  
840 Oceans*, 115, 1978 - 2012, 2010.

841 Huang, X., Song, Y., Li, M. M., Li, J. F., Huo, Q., Cai, X. H., Zhu, T., Hu, M., and  
842 Zhang, H. S.: A high-resolution ammonia emission inventory in China, *Global Biogeochem  
843 Cy*, 26, GB1030, doi:10.1029/2011GB004161, 2012.

844 [Huijnen, V., Eskes, H. J., Poupkou, A., Elbern, H., Boersma, K. F., Foret, G., Sofiev, M.,  
845 Valdebenito, A., Flemming, J., Stein, O., Gross, A., Robertson, L., D'Isidoro, M.,  
846 Kioutsioukis, I., Friese, E., Amstrup, B., Bergstrom, R., Strunk, A., Vira, J., Zyryanov, D.,  
847 Maurizi, A., Melas, D., Peuch, V. H., and Zerefos, C.: Comparison of OMI NO<sub>2</sub> tropospheric  
848 columns with an ensemble of global and European regional air quality models, \*Atmos. Chem.  
849 Phys.\*, 10, 3273-3296, 2010.](#)

850 Hyvonen, R., Persson, T., Andersson, S., Olsson, B., Agren, G. I., and Linder, S.: Impact  
851 of long-term nitrogen addition on carbon stocks in trees and soils in northern Europe,  
852 *Biogeochemistry*, 89, 121-137, 2008.

853 [Jia, Y., Yu, G., He, N., Zhan, X., Fang, H., Sheng, W., Zuo, Y., Zhang, D., and Wang,  
854 Q.: Spatial and decadal variations in inorganic nitrogen wet deposition in China induced by  
855 human activity, \*Scientific reports\*, 4, 3763, 10.1038/srep03763, 2014.](#)

856 Jiang, Z., Jones, D. B. A., Worden, J. R., Worden, H. M., Henze, D. K., Wang, Y. X.,  
857 Regional data assimilation of multi-spectral MOPITT observations of CO over North  
858 America, *Atmos. Chem. Phys.*, *Atmos. Chem. Phys. Discuss.*, 15, 5327-5358,  
859 doi:10.5194/acpd-15-5327-2015, 2015.

860 Jung, J., Furutani, H., Uematsu, M.: Atmospheric inorganic nitrogen in marine aerosol  
861 and precipitation and its deposition to the North and South Pacific Oceans, *J. Atmos. Chem.*,  
862 68, 157-181, 2011.

863 Kim, P. S., Jacob, D. J., Mickley, L. J., Koplitz, S. N., Marlier, M. E., DeFries, R. S.,  
864 Myers, S. S., Chew, B. N., and Mao, Y. H.: Sensitivity of population smoke exposure to fire

865 locations in Equatorial Asia, *Atmos. Environ.*, 102, 11-17, 2015.

866 Kim, T. W., Lee, K., Najjar, R. G., Jeong, H. D., and Jeong, H. J.: Increasing N  
867 Abundance in the Northwestern Pacific Ocean Due to Atmospheric Nitrogen Deposition,  
868 *Science*, 334, 505-509, 2011.

869 Kim, T. W., Lee, K., Duce, R., and Liss, P.: Impact of atmospheric nitrogen deposition  
870 on phytoplankton productivity in the South China Sea, *Geophys. Res. Lett.*, 41, 3156-3162,  
871 2014.

872 Kopacz, M., Jacob, D. J., Henze, D. K., Heald, C. L., Streets, D. G., and Zhang, Q.:  
873 Comparison of adjoint and analytical Bayesian inversion methods for constraining Asian  
874 sources of carbon monoxide using satellite (MOPITT) measurements of CO columns, *J.*  
875 *Geophys. Res.-Atmos.*, 114, D04305, doi:10.1029/2007JD009264, 2009.

876 [Koracin, D., and Berkowicz, R.: Nocturnal boundary-layer height: Observations by](#)  
877 [acoustic sounders and predictions in terms of surface-layer parameters, \*Boundary-Layer\*](#)  
878 [Meteorol.](#), 43, 65-83, 1988.

879 Kurokawa, J., Ohara, T., Morikawa, T., Hanayama, S., Janssens-Maenhout, G., Fukui, T.,  
880 Kawashima, K., and Akimoto, H.: Emissions of air pollutants and greenhouse gases over  
881 Asian regions during 2000-2008: Regional Emission inventory in ASia (REAS) version 2,  
882 *Atmos. Chem. Phys.*, 13, 11019-11058, doi:10.5194/acp-13-11019-2013, 2013.

883 [Lamsal, L. N., Martin, R. V., van Donkelaar, A., Celarier, E. A., Bucsela, E. J., Boersma,](#)  
884 [K. F., Dirksen, R., Luo, C., and Wang, Y.: Indirect validation of tropospheric nitrogen dioxide](#)  
885 [retrieved from the OMI satellite instrument: Insight into the seasonal variation of nitrogen](#)  
886 [oxides at northern midlatitudes, \*J. Geophys. Res.\*, 115, D05302, 10.1029/2009jd013351,](#)  
887 [2010.](#)

888 Levelt, P. F., Hilsenrath, E., Leppelmeier, G. W., van den Oord, G. H. J., Bhartia, P. K.,  
889 Tamminen, J., de Haan, J. F., and Veefkind, J. P.: Science objectives of the Ozone Monitoring  
890 Instrument, *IEEE T. Geosci. Remote*, 44, 1199-1208, 2006.

891 Liang, Q., Jaeglé, L., Jaffe, D. A., Weiss-Penzias, P., Heckman, A., Snow, J. A.:  
892 Long-range transport of Asian pollution to the northeast Pacific: Seasonal variations and  
893 transport pathways of carbon monoxide, *J. Geophys. Res.*, 109, D23S07,  
894 doi:10.1029/2003JD004402, 2004.

895 Liao, J.: Fertilizer application and analysis, Shanghai science and Technology Press,  
896 Shanghai, 1993.

897 Lin, J. T., Martin, R. V., Boersma, K. F., Sneep, M., Stammes, P., Spurr, R., Wang, P.,  
898 Van Roozendaal, M., Clemer, K., and Irie, H.: Retrieving tropospheric nitrogen dioxide from  
899 the Ozone Monitoring Instrument: effects of aerosols, surface reflectance anisotropy, and  
900 vertical profile of nitrogen dioxide, *Atmos. Chem. Phys.*, 14, 1441-1461,  
901 doi:10.5194/acp-14-1441-2014, 2014.

902 Liu, H. Y., Jacob, D. J., Bey, I., and Yantosca, R. M.: Constraints from Pb-210 and Be-7  
903 on wet deposition and transport in a global three-dimensional chemical tracer model driven by  
904 assimilated meteorological fields, *J. Geophys. Res.*, 106, 12109-12128, 2001.

905 Liu, H. Y., Jacob, D. J., Bey, I., Yantosca, R. M., Duncan, B. N., and Sachse, G. W.:  
906 Transport pathways for Asian pollution outflow over the Pacific: Interannual and seasonal  
907 variations, *J. Geophys. Res.-Atmos.*, 108, 8786, doi:10.1029/2002JD003102, 2003.

908 Liu, X. J., Zhang, Y., Han, W. X., Tang, A. H., Shen, J. L., Cui, Z. L., Vitousek, P.,

909 Erisman, J. W., Gouling, K., Christie, P., Fangmeier, A., and Zhang, F. S.: Enhanced  
910 nitrogen deposition over China, *Nature*, 494, 459-462, 2013.

911 Luo, X. S., Tang, A. H., Shi, K., Wu, L. H., Li, W. Q., Shi, W. Q., Shi, X. K., Erisman, J.  
912 W., Zhang, F. S., and Liu, X. J.: Chinese coastal seas are facing heavy atmospheric nitrogen  
913 deposition, *Environ. Res. Lett.*, 9, 095007, doi:10.1088/1748-9326/9/9/095007, 2014.

914 Lv, C. Q., and Tian, H. Q.: Spatial and temporal patterns of nitrogen deposition in China:  
915 Synthesis of observational data, *J. Geophys. Res.-Atmos.*, 112, D22S05,  
916 doi:10.1029/2006JD007990, 2007.

917 Mao, J., Jacob, D. J., Evans, M. J., Olson, J. R., Ren, X., Brune, W. H., St Clair, J. M.,  
918 Crounse, J. D., Spencer, K. M., Beaver, M. R., Wennberg, P. O., Cubison, M. J., Jimenez, J.  
919 L., Fried, A., Weibring, P., Walega, J. G., Hall, S. R., Weinheimer, A. J., Cohen, R. C., Chen,  
920 G., Crawford, J. H., McNaughton, C., Clarke, A. D., Jaegle, L., Fisher, J. A., Yantosca, R. M.,  
921 Le Sager, P., and Carouge, C.: Chemistry of hydrogen oxide radicals (HOx) in the Arctic  
922 troposphere in spring, *Atmos. Chem. Phys.*, 10, 5823-5838, doi:10.5194/acp-10-5823-2010,  
923 2010.

924 Mao, Y. H., Li, Q. B., Henze, D. K., Jiang, Z., Jones, D. B. A., Kopacz, M., He, C., Qi,  
925 L., Gao, M., Hao, W.-M., and Liou, K.-N.: Variational estimates of black carbon emissions in  
926 the western United States, *Atmos. Chem. Phys. Discuss.*, 14, 21865-21916,  
927 doi:10.5194/acpd-14-21865-2014, 2014.

928 Mari, C., Jacob, D. J., and Bechtold, P.: Transport and scavenging of soluble gases in a  
929 deep convective cloud, *J. Geophys. Res.-Atmos.*, 105, 22255-22267, 2000.

930 Martin, R. V., Jacob, D. J., Chance, K., Kurosu, T. P., Palmer, P. I., Evans, M. J.: Global  
931 inventory of nitrogen oxide emissions constrained by space-based observations of NO<sub>2</sub>  
932 columns, *J. Geophys. Res.*, 108, 4537, doi:10.1029/2003JD003453, 2003.

933 Martin, R. V., Sauvage, B., Folkens, I., Sioris, C. E., Boone, C., Bernath, P., and Ziemke,  
934 J.: Space-based constraints on the production of nitric oxide by lightning, *J. Geophys.*  
935 *Res.-Atmos.*, 112, D09309, doi:10.1029/2006jd007831, 2007.

936 Monfreda, C., Ramankutty, N., and Foley, J. A.: Farming the planet: 2. Geographic  
937 distribution of crop areas, yields, physiological types, and net primary production in the year  
938 2000, *Global Biogeochem. Cy.*, 22, GB1022, doi:10.1029/2007GB002947, 2008.

939 Murray, L. T., Jacob, D. J., Logan, J. A., Hudman, R. C., and Koshak, W. J.: Optimized  
940 regional and interannual variability of lightning in a global chemical transport model  
941 constrained by LIS/OTD satellite data, *J. Geophys. Res.-Atmos.*, 117, D20307,  
942 doi:10.1029/2012JD017934, 2012.

943 O'Byrne, G., Martin, R. V., van Donkelaar, A., Joiner, J., and Celarier, E. A.: Surface  
944 reflectivity from the Ozone Monitoring Instrument using the Moderate Resolution Imaging  
945 Spectroradiometer to eliminate clouds: Effects of snow on ultraviolet and visible trace gas  
946 retrievals, *J. Geophys. Res.*, 115, D17305, doi:10.1029/2009JD013079, 2010.

947 Olivier, J. G. J. and Berndowski, J. J. M.: Global emissions sources and sinks, in: *The*  
948 *Climate System*, edited by: Berndowski, J., Guicherit, R., and Heij, B. J., 33-78, A. A.  
949 Balkema Publishers/Swets & Zeitlinger Publishers, Lisse, The Netherlands, ISBN: 90 5809  
950 255 0, 2001.

951 Pan, Y. P., Wang, Y. S., Tang, G. Q., and Wu, D.: Wet and dry deposition of  
952 atmospheric nitrogen at ten sites in Northern China, *Atmos. Chem. Phys.*, 12, 6515-6535,

953 doi:10.5194/acp-12-6515-2012, 2012.

954 Park, R. J., Jacob, D. J., Field, B. D., Yantosca, R. M., and Chin, M.: Natural and  
955 transboundary pollution influences on sulfate-nitrate-ammonium aerosols in the United States:  
956 Implications for policy, *J. Geophys. Res.-Atmos.*, 109, D15204, doi:10.1029/2003JD004473,  
957 2004.

958 Paulot, F., Jacob, D. J., and Henze, D. K.: Sources and Processes Contributing to  
959 Nitrogen Deposition: An Adjoint Model Analysis Applied to Biodiversity Hotspots  
960 Worldwide, *Environ. Sci. Technol.*, 47, 3226-3233, 2013.

961 Paulot, F., Jacob, D. J., Pinder, R. W., Bash, J. O., Travis, K., and Henze, D. K.:  
962 Ammonia emissions in the United States, European Union, and China derived by  
963 high-resolution inversion of ammonium wet deposition data: Interpretation with a new  
964 agricultural emissions inventory (MASAGE\_NH3), *J. Geophys. Res.-Atmos.*, 119, 4343-4364,  
965 2014.

966 [Paulot, F., Jacob, D. J., Johnson, M. T., Bell, T. G., Baker, A. R., Keene, W. C., Lima, I.  
967 D., Doney, S. C., and Stock, C. A.: Global oceanic emission of ammonia: Constraints from  
968 seawater and atmospheric observations, \*Global Biogeochem. Cycles\*, 29,  
969 doi:10.1002/2015GB005106, 2015.](#)

970 Pickering, K. E., Wang, Y. S., Tao, W. K., Price, C., and Muller, J. F.: Vertical  
971 distributions of lightning NO<sub>x</sub> for use in regional and global chemical transport models, *J.  
972 Geophys. Res.-Atmos.*, 103, 31203-31216, 1998.

973 Pinder, R. W., Adams, P. J., Pandis, S. N., and Gilliland, A. B.: Temporally resolved  
974 ammonia emission inventories: Current estimates, evaluation tools, and measurement needs, *J.  
975 Geophys. Res.-Atmos.*, 111, D16310, doi:10.1029/2005jd006603, 2006.

976 Price, C., and Rind, D.: A Simple Lightning Parameterization for Calculating Global  
977 Lightning Distributions, *J. Geophys. Res.-Atmos.*, 97, 9919-9933, 1992.

978 Pregitzer, K. S., Burton, A. J., Zak, D. R., and Talhelm, A. F.: Simulated chronic  
979 nitrogen deposition increases carbon storage in Northern Temperate forests, *Glob. Change  
980 Biol.*, 14, 142-153, 2008.

981 Rodgers, C. D.: Inverse methods for atmospheric sounding-Theory and practise, edited  
982 by: Taylor, F. W., World Scientific, Singapore, 2000.

983 Sacks, W. J., Deryng, D., Foley, J. A., and Ramankutty, N.: Crop planting dates: an  
984 analysis of global patterns, *Global Ecol. Biogeogr.*, 19, 607-620, 2010.

985 Sanderson, M. G., Dentener, F. J., Fiore, A. M., Cuvelier, C., Keating, T. J., Zuber, A.,  
986 Atherton, C. S., Bergmann, D. J., Diehl, T., Doherty, R. M., Duncan, B. N., Hess, P.,  
987 Horowitz, L. W., Jacob, D. J., Jonson, J. E., Kaminski, J. W., Lupu, A., MacKenzie, I. A.,  
988 Mancini, E., Marmer, E., Park, R., Pitari, G., Prather, M. J., Pringle, K. J., Schroeder, S.,  
989 Schultz, M. G., Shindell, D. T., Szopa, S., Wild, O., and Wind, P.: A multi-model study of the  
990 hemispheric transport and deposition of oxidised nitrogen, *Geophys. Res. Lett.*, 35, L17815,  
991 doi:10.1029/2008GL035389, 2008.

992 Sauvage, B., Martin, R. V., van Donkelaar, A., Liu, X., Chance, K., Jaegle, L., Palmer, P.  
993 I., Wu, S., and Fu, T. M.: Remote sensed and in situ constraints on processes affecting  
994 tropical tropospheric ozone, *Atmos. Chem. Phys.*, 7, 815-838, doi:10.5194/acp-7-815-2007,  
995 2007.

996 Seitzinger, S., Harrison, J. A., Bohlke, J. K., Bouwman, A. F., Lowrance, R., Peterson,

997 B., Tobias, C., and Van Drecht, G.: Denitrification across landscapes and waterscapes: A  
998 synthesis, *Ecol. Appl.*, 16, 2064-2090, 2006.

999 Shephard, M. W., Cady-Pereira, K. E., Luo, M., Henze, D. K., Pinder, R. W., Walker, J.  
1000 T., Rinsland, C. P., Bash, J. O., Zhu, L., Payne, V. H., and Clarisse, L.: TES ammonia  
1001 retrieval strategy and global observations of the spatial and seasonal variability of ammonia,  
1002 *Atmos. Chem. Phys.*, 11, 10743-10763, doi:10.5194/acp-11-10743-2011, 2011.

1003 Skjøth, C. A., Geels, C., Berge, H., Gyldenkaerne, S., Fagerli, H., Ellermann, T., Frohn,  
1004 L. M., Christensen, J., Hansen, K. M., Hansen, K., and Hertel, O.: Spatial and temporal  
1005 variations in ammonia emissions - a freely accessible model code for Europe, *Atmos. Chem.*  
1006 *Phys.*, 11, 5221-5236, doi:10.5194/acp-11-5221-2011, 2011.

1007 Stevens, C. J., Dise, N. B., Mountford, J. O., and Gowing, D. J.: Impact of nitrogen  
1008 deposition on the species richness of grasslands, *Science*, 303, 1876-1879, 2004.

1009 Streets, D. G., Bond, T. C., Carmichael, G. R., Fernandes, S. D., Fu, Q., He, D., Klimont,  
1010 Z., Nelson, S. M., Tsai, N. Y., Wang, M. Q., Woo, J. H., and Yarber, K. F.: An inventory of  
1011 gaseous and primary aerosol emissions in Asia in the year 2000, *J. Geophys. Res.-Atmos.*,  
1012 108, 8809, doi:10.1029/2002JD003093, 2003.

1013 [Sutton, M. A., Burkhardt, J. K., Guerin, D., Nemitz, E., and Fowler, D.: Development of](#)  
1014 [resistance models to describe measurements of bi-directional ammonia surface-atmosphere](#)  
1015 [exchange, \*Atmos. Environ.\*, 32, 473-480, 1998.](#)

1016 van der Werf, G. R., Randerson, J. T., Giglio, L., Collatz, G. J., Kasibhatla, P. S., and  
1017 Arellano, A. F.: Interannual variability in global biomass burning emissions from 1997 to  
1018 2004, *Atmos. Chem. Phys.*, 6, 3423-3441, doi:10.5194/acp-6-3423-2006, 2006.

1019 Vestreng, V. and Klein, H.: Emission data reported to UNECE/EMEP: Quality assurance  
1020 and trend analysis & Presentation of WebDab, MSC-W Status Report 2002, Norwegian  
1021 Meteorological Institute, Oslo, 2002.

1022 Vinken, G. C. M., Boersma, K. F., Jacob, D. J., and Meijer, E. W.: Accounting for  
1023 non-linear chemistry of ship plumes in the GEOS-Chem global chemistry transport model,  
1024 *Atmos. Chem. Phys.*, 11, 11707-11722, doi:10.5194/acp-11-11707-2011, 2011.

1025 Wang, J., Hoffmann, A. A., Park, R. J., Jacob, D. J., and Martin, S. T.: Global  
1026 distribution of solid and aqueous sulfate aerosols: Effect of the hysteresis of particle phase  
1027 transitions, *J. Geophys. Res.*, 113, D11206, doi:10.1029/2007JD009367, 2008.

1028 Wang, Y. H., Jacob, D. J., Logan, J. A.: Global simulation of tropospheric  
1029 O<sub>3</sub>-NO<sub>x</sub>-hydrocarbon chemistry, 3. Origins of tropospheric ozone and effects of  
1030 nonmethane hydrocarbons, *J. Geophys. Res.*, 103, 10757-10767, 1998.

1031 [Wang, Y., Zhang, Q. Q., He, K., Zhang, Q., and Chai, L.: Sulfate-nitrate-ammonium](#)  
1032 [aerosols over China: response to 2000-2015 emission changes of sulfur dioxide, nitrogen](#)  
1033 [oxides, and ammonia, \*Atmos. Chem. Phys.\*, 13, 2635-2652, 2013.](#)

1034 Wesely, M. L.: Parameterization of Surface Resistances to Gaseous Dry Deposition in  
1035 Regional-Scale Numerical-Models, *Atmos. Environ.*, 23, 1293-1304, 1989.

1036 Xie, P. P., and Arkin, P. A.: Global precipitation: A 17-year monthly analysis based on  
1037 gauge observations, satellite estimates, and numerical model outputs, *B. Am. Meteorol. Soc.*,  
1038 78, 2539-2558, 1997.

1039 Yienger, J. J., and Levy, H.: Empirical-Model of Global Soil-Biogenic NO<sub>x</sub> Emissions, *J.*  
1040 *Geophys. Res.-Atmos.*, 100, 11447-11464, 1995.



1041 Zhang, B., Owen, R. C., Perlinger, J. A., Kumar, A., Wu, S., Martin, M. V., Kramer, L.,  
1042 Helmig, D., and Honrath, R. E.: A semi-Lagrangian view of ozone production tendency in  
1043 North American outflow in the summers of 2009 and 2010, *Atmos. Chem. Phys.*, 14,  
1044 2267-2287, doi:10.5194/acp-14-2267-2014, 2014.

1045 Zhang, L., Jacob, D. J., Bowman, K. W., Logan, J. A., Turquety, S., Hudman, R. C., Li,  
1046 Q. B., Beer, R., Worden, H. M., Worden, J. R., Rinsland, C. P., Kulawik, S. S., Lampel, M. C.,  
1047 Shephard, M. W., Fisher, B. M., Eldering, A., and Avery, M. A.: Ozone-CO correlations  
1048 determined by the TES satellite instrument in continental outflow regions, *Geophys. Res.*  
1049 *Let.*, 33, L18804, doi:10.1029/2006GL026399, 2006.

1050 Zhang, L., Jacob, D. J., Kopacz, M., Henze, D. K., Singh, K., and Jaffe, D. A.:  
1051 Intercontinental source attribution of ozone pollution at western U.S. sites using an adjoint  
1052 method, *Geophys. Res. Let.*, 36, L11810, doi:10.1029/2009GL037950, 2009.

1053 Zhang, L., Liao, H., and Li, J.: Impacts of Asian summer monsoon on seasonal and  
1054 interannual variations of aerosols over eastern China, *J. Geophys. Res.*, 115, D00K05,  
1055 doi:10.1029/2009JD012299, 2010.

1056 Zhang, L., Jacob, D. J., Knipping, E. M., Kumar, N., Munger, J. W., Carouge, C. C., van  
1057 Donkelaar, A., Wang, Y. X., and Chen, D.: Nitrogen deposition to the United States:  
1058 distribution, sources, and processes, *Atmos. Chem. Phys.*, 12, 4539-4554,  
1059 doi:10.5194/acp-12-4539-2012, 2012.

1060 [Zhang, L., Jacob, D. J., Yue, X., Downey, N. V., Wood, D. A., and Blewitt, D.: Sources](#)  
1061 [contributing to background surface ozone in the US Intermountain West, \*Atmos. Chem. Phys.\*,](#)  
1062 [14, 5295-5309, 10.5194/acp-14-5295-2014, 2014.](#)

1063 [Zhang, L., Liu, L., Zhao, Y., Gong, S., Zhang, X., Henze, D. K., Capps, S. L., Fu, T.-M.,](#)  
1064 [Zhang, Q., and Wang, Y.: Source attribution of particulate matter pollution over North China](#)  
1065 [with the adjoint method, \*Environmental Research Letters\*, 10, 084011,](#)  
1066 [10.1088/1748-9326/10/8/084011, 2015.](#)

1067 Zhang, Q., Streets, D. G., Carmichael, G. R., He, K. B., Huo, H., Kannari, A., Klimont,  
1068 Z., Park, I. S., Reddy, S., Fu, J. S., Chen, D., Duan, L., Lei, Y., Wang, L. T., and Yao, Z. L.:  
1069 Asian emissions in 2006 for the NASA INTEX-B mission, *Atmos. Chem. Phys.*, 9,  
1070 5131-5153, doi:10.5194/acp-9-5131-2009, 2009.

1071 [Zhang, Y., Yu, Q., Ma, W. C., and Chen, L. M.: Atmospheric deposition of inorganic](#)  
1072 [nitrogen to the eastern China seas and its implications to marine biogeochemistry, \*J. Geophys.\*](#)  
1073 [Res.-Atmos.](#), 115, D00K10, doi:10.1029/2009JD012814, 2010.

1074 [Zhu, J., He, N., Wang, Q., Yuan, G., Wen, D., Yu, G., and Jia, Y.: The composition,](#)  
1075 [spatial patterns, and influencing factors of atmospheric wet nitrogen deposition in Chinese](#)  
1076 [terrestrial ecosystems, \*Sci. Total Environ.\*, 511, 777-785, 2015a.](#)

1077 Zhu, L., Henze, D. K., Cady-Pereira, K. E., Shephard, M. W., Luo, M., Pinder, R. W.,  
1078 Bash, J. O., and Jeong, G. R.: Constraining U.S. ammonia emissions using TES remote  
1079 sensing observations and the GEOS-Chem adjoint model, *J. Geophys. Res.-Atmos.*, 118,  
1080 3355-3368, 2013.

1081 [Zhu, L., Henze, D., Bash, J., Jeong, G.-R., Cady-Pereira, K., Shephard, M., Luo, M.,](#)  
1082 [Paulot, F., and Capps, S.: Global evaluation of ammonia bi-directional exchange, \*Atmos.\*](#)  
1083 [Chem. Phys. Discuss.](#), 15, 4823-4877, doi:10.5194/acpd-15-4823-2015, 2015b.

1084



1086 **Tables**

1087

1088 **Table 1.** Monthly mean daytime dry deposition velocities over the northwestern

1089 Pacific<sup>a</sup>

	January	April	July	October
NH <sub>3</sub>	1.10	0.70	0.60	0.85
Aerosol NH <sub>4</sub> <sup>+</sup>	0.08	0.06	0.06	0.07
HNO <sub>3</sub> , Isoprene nitrates <sup>b</sup>	1.16	0.69	0.56	0.84
Aerosol NO <sub>3</sub> <sup>-</sup>	0.08	0.06	0.06	0.07
N <sub>2</sub> O <sub>5</sub>	1.16	0.69	0.56	0.84
NO <sub>2</sub>	0.01	0.01	0.01	0.01
PANs <sup>c</sup>	0.01	0.01	0.01	0.01

1090 <sup>a</sup> Numbers are in unit of cm s<sup>-1</sup> and averaged over 2008-2010.

1091 <sup>b</sup> Isoprene nitrates represent the organic nitrates produced from the oxidation of  
1092 isoprene by OH in the presence of NO<sub>x</sub>.

1093 <sup>c</sup> Peroxyacetyl nitrate (PAN) and higher peroxyacyl nitrates.

1094

1095

1096 **Table 2. Annual total NH<sub>3</sub> and NO<sub>x</sub> emissions over Asia and China<sup>a</sup>**

Source type		Asia	China
NH <sub>3</sub>	Fertilizer	15.5	7.8
	Livestock	5.1	2.4
	Human waste	4.0	1.5
	Others <sup>b</sup>	1.8	0.7
	Natural <sup>c</sup>	2.1 (0.5) <sup>d</sup>	0.5
Total		28.6	12.8
NO <sub>x</sub>	Power plants	4.1	2.8
	Transport	4.8	1.8
	Industry	2.8	2.0
	Domestic	1.3	0.7
	Natural <sup>e</sup>	2.6	0.7
Total		15.7	7.9

1097 <sup>a</sup> Annual emissions in unit of Tg N a<sup>-1</sup> for 2008-2010.

1098 <sup>b</sup> Other anthropogenic sources include ammonia emissions from power plant,  
1099 transport, industry, and domestic emission.

1100 <sup>c</sup> Natural NH<sub>3</sub> emissions include emissions from natural terrestrial and ocean.

1101 <sup>d</sup> [Annual NH<sub>3</sub> oceanic emissions over this region.](#)

1102 <sup>e</sup> [Natural NO<sub>x</sub> emissions include emissions from soil, lightning and biomass burning.](#)

1103

lin zhang 15/9/1 11:28 AM

已删除: <sup>d</sup>

lin zhang 15/9/1 11:29 AM

已删除:

lin zhang 15/9/1 11:29 AM

已删除: <sup>d</sup>

1107

1108

1109

1110 **Table 3. Monthly and annual nitrogen deposition fluxes to the Yellow Sea and**  
 1111 **the South China Sea for 2008-2010<sup>a</sup>**

	Wet deposition		Dry deposition		Total	
	NH <sub>4</sub> <sup>+</sup>	NO <sub>3</sub> <sup>-</sup>	NH <sub>x</sub>	NO <sub>y</sub>		
<b>The Yellow Sea</b>	January	0.24 (0.16-0.27)	0.38 (0.25-0.47)	0.05 (0.05-0.06)	0.45 (0.45-0.45)	1.12 (0.92-1.25)
	April	0.35 (0.21-0.46)	0.27 (0.18-0.37)	0.10 (0.07-0.12)	0.14 (0.13-0.15)	0.85 (0.63-1.08)
	July	0.48 (0.40-0.60)	0.36 (0.30-0.43)	0.08 (0.06-0.11)	0.13 (0.11-0.15)	1.04 (0.89-1.28)
	October	0.34 (0.20-0.53)	0.32 (0.21-0.46)	0.12 (0.07-0.17)	0.29 (0.22-0.38)	1.07 (0.71-1.54)
	Annual	4.1 (3.8-4.2)	3.9 (3.9-3.9)	0.9 (0.8-1.0)	3.0 (2.8-3.1)	11.9 (11.3-12.3)
<b>The South China Sea</b>	January	0.18 (0.13-0.24)	0.17 (0.12-0.21)	0.03 (0.02-0.04)	0.23 (0.15-0.34)	0.62 (0.43-0.83)
	April	0.20 (0.14-0.26)	0.12 (0.08-0.16)	0.04 (0.04-0.05)	0.08 (0.07-0.09)	0.43 (0.34-0.56)
	July	0.10 (0.04-0.14)	0.09 (0.05-0.11)	0.02 (0.01-0.02)	0.02 (0.01-0.02)	0.23 (0.11-0.29)
	October	0.20 (0.16-0.24)	0.16 (0.13-0.22)	0.05 (0.04-0.07)	0.13 (0.10-0.18)	0.54 (0.42-0.63)
	Annual	2.1 (1.8-2.3)	1.7 (1.5-1.8)	0.4 (0.4-0.5)	1.4 (1.2-1.5)	5.6 (4.8-6.1)

1112

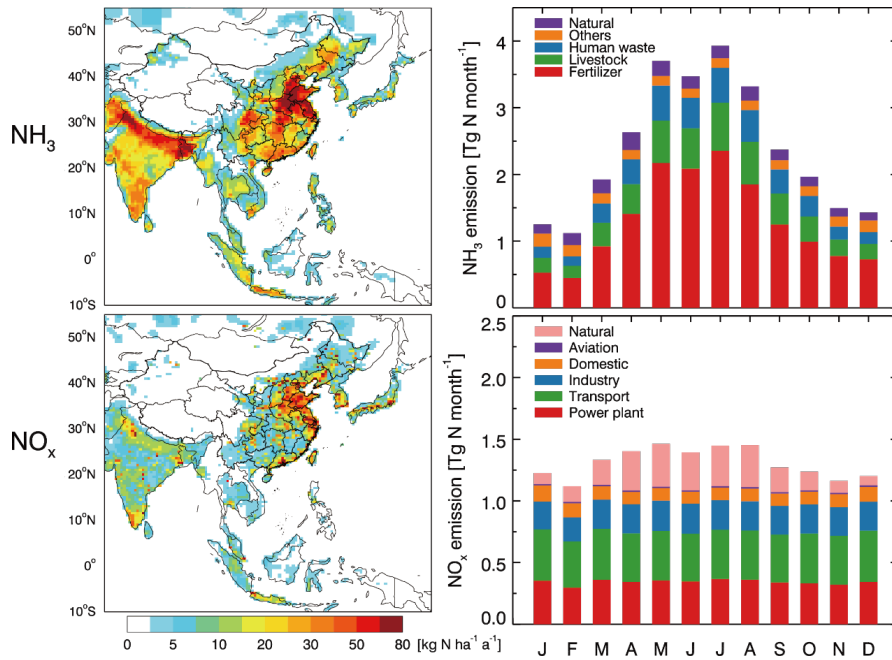
1113 <sup>a</sup>Numbers are three-year (2008-2010) averages and ranges (in parentheses) in unit of  
 1114 kg N ha<sup>-1</sup> month<sup>-1</sup> for the monthly values and kg N ha<sup>-1</sup> a<sup>-1</sup> for the annual totals.

1115

1116

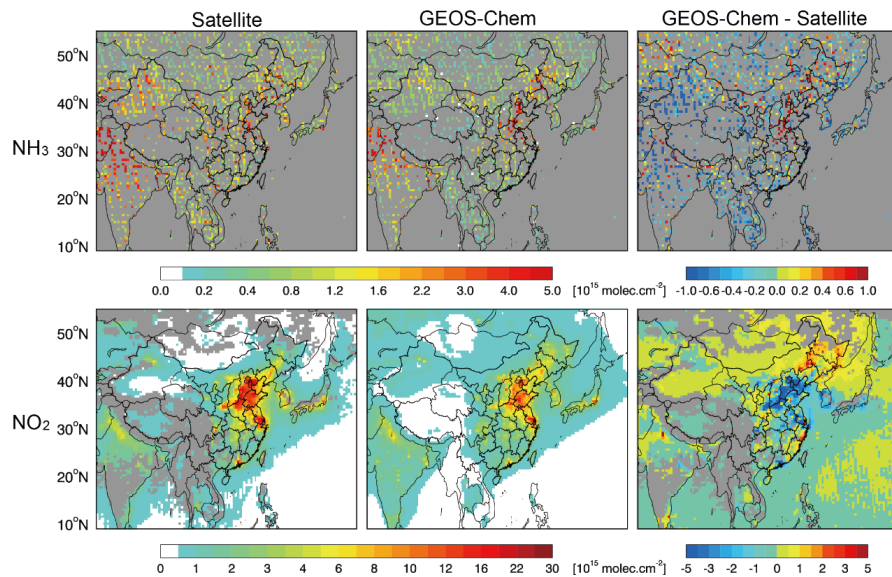
1117

1118 **Figures**  
1119



1120  
1121  
1122  
1123  
1124  
1125  
1126  
1127

**Fig. 1.** Asian  $\text{NH}_3$  and  $\text{NO}_x$  emissions in 2008-2010. The left panels show annual total emissions and the right panels show monthly values of  $\text{NH}_3$  and  $\text{NO}_x$  emissions from each source type over Asia.

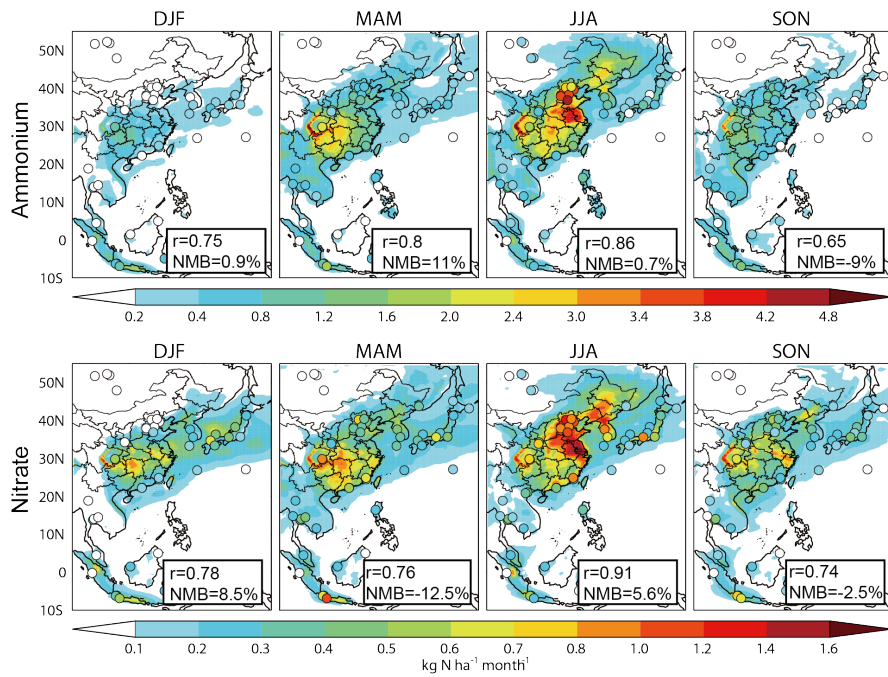


1128

1129 **Fig. 2.** Satellite observations of  $\text{NH}_3$  tropospheric columns from TES (top left) and  
 1130  $\text{NO}_2$  tropospheric columns from OMI (bottom left). The TES observations are  
 1131 daytime measurements during June-August 2005-2010. The OMI observations during  
 1132 March-November 2009 are from KNMI at  $0.125^\circ \times 0.125^\circ$  resolution. Both are  
 1133 regridded to the model resolution ( $1/2^\circ \times 2/3^\circ$ ). The middle panels show corresponding  
 1134 GEOS-Chem model results for 2009 sampled at the satellite overpass time (13:45  
 1135 local time). The right panels show the GEOS-Chem minus satellite differences.

1136

1137



1138

1139 **Fig. 3.** GEOS-Chem simulated seasonal mean ammonium (top panels) and nitrate  
 1140 (bottom panels) wet deposition fluxes for 2008-2010. The measurements from  
 1141 EANET (49 sites in the domain) and ten CAS sites are over-plotted (circles).  
 1142 Correlation coefficients ( $r$ ) and mean normalized biases (NMB) are given inset. The  
 1143 EANET data and model results are averaged for January 2008-December 2010, and  
 1144 the CAS data are for December 2007-November 2010. DJF represents  
 1145 December-Januray-Februray, MAM: March-April-May, JJA: June-July-August, SON:  
 1146 September-October-November.

1147

1148

1149

1150

1151

1152

1153

1154

1155

1156

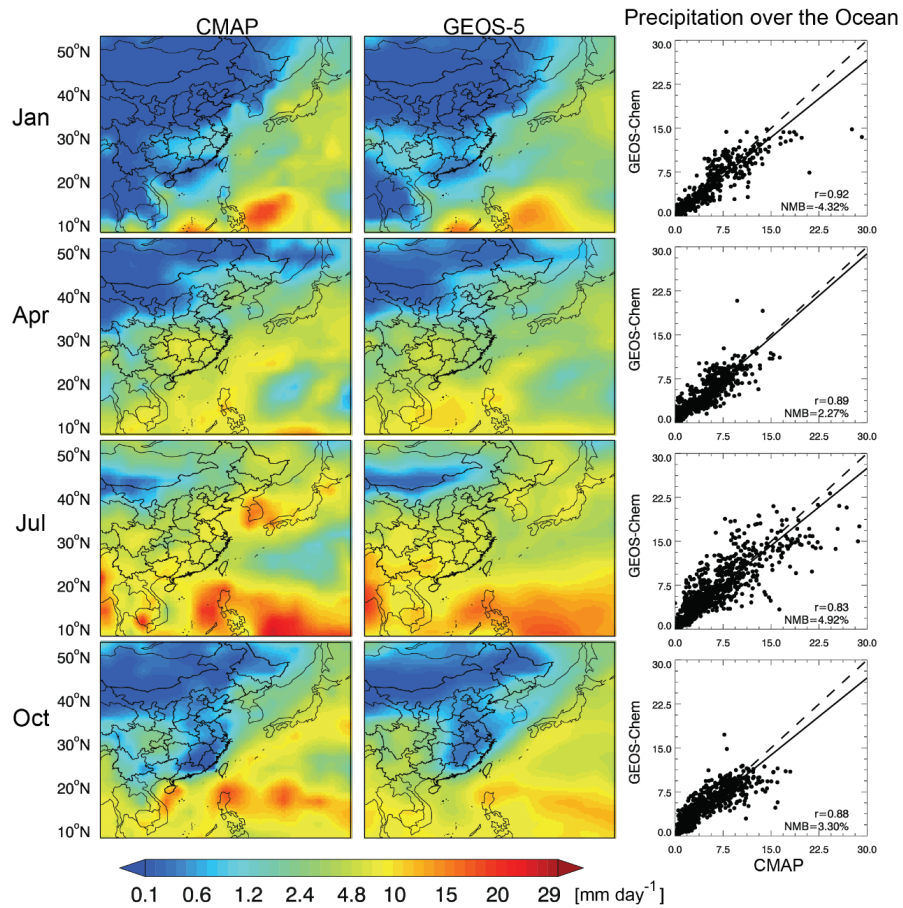
1157

1158

1159

1160

1161



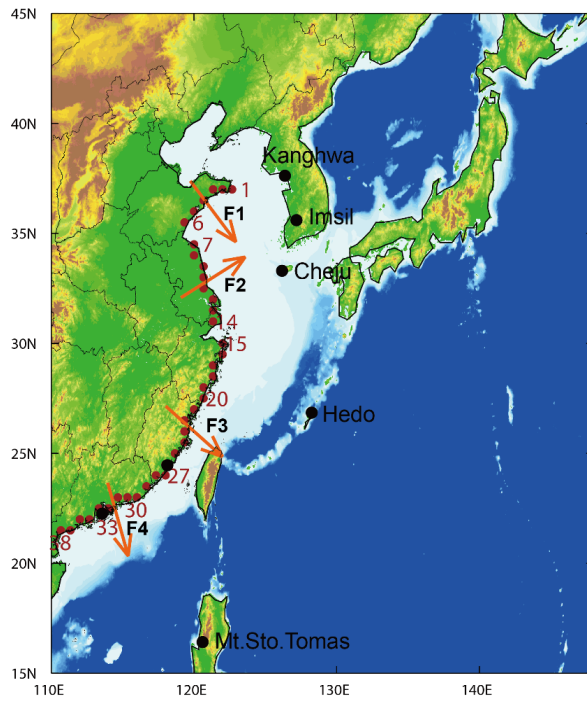
1162

1163

1164 **Fig. 4.** Monthly mean precipitation data from CMAP (left panels) and from GEOS-5  
 1165 (central panels) for January, April, July and October 2009. The right panels show  
 1166 corresponding scatter-plots of CMAP versus GEOS-5 precipitation over the  
 1167 northwestern Pacific Ocean. Correlation coefficients ( $r$ ) and mean normalized biases  
 1168 (NMB) are shown inset.

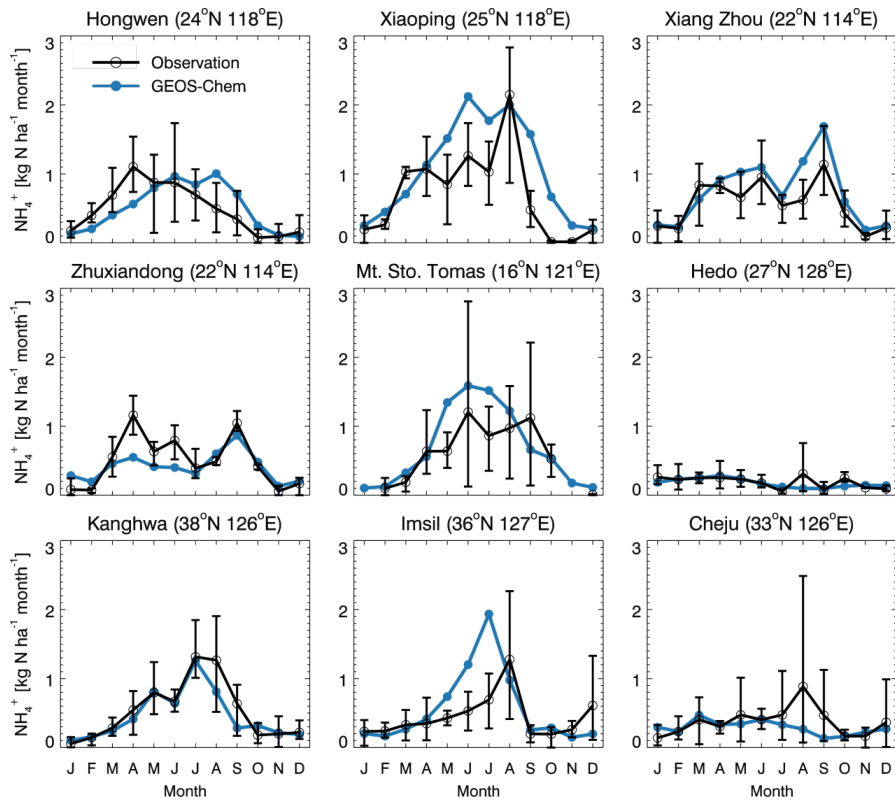
1169





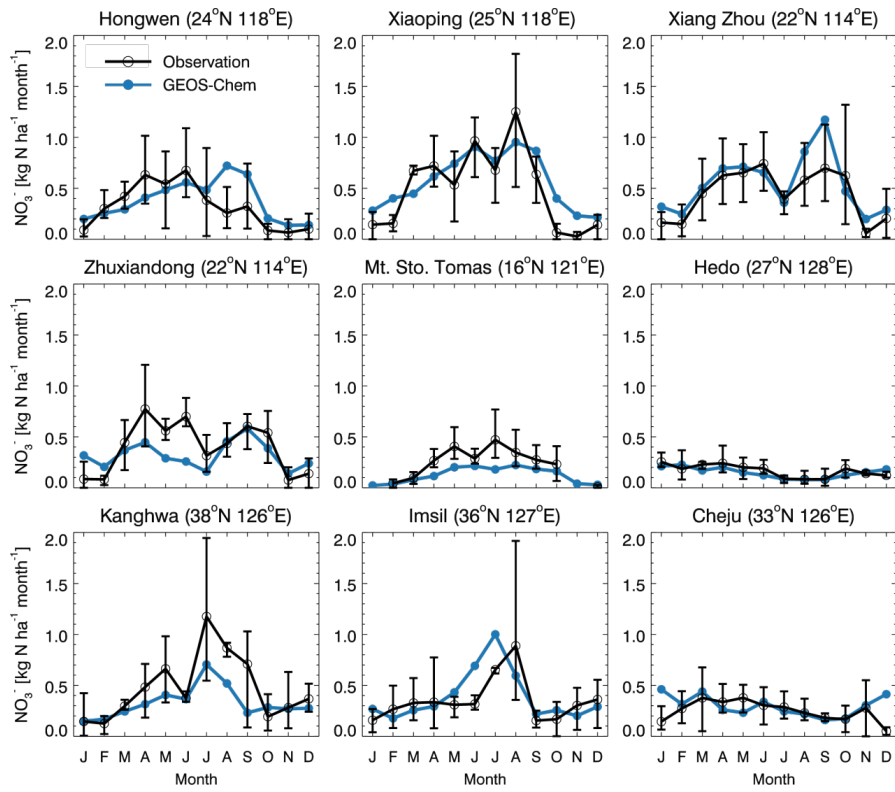
1170  
 1171  
 1172  
 1173  
 1174  
 1175  
 1176  
 1177  
 1178

**Fig. 5.** Map of the focused domain. The black dots are the locations of nine EANET sites that used for model evaluation of nitrogen deposition near the coast (Figure 6a and 6b): Mt. St. Tomas, Hedo, Cheju, Imsil, Kanghwa, Xiamen (Hongwen and Xiaoping sites), and Zhuhai (Xiang Zhou and Zhuxiandong sites). The red dots represent the grid cells covering the coastline of Mainland China that used for determining the outflow fluxes as indicated by the orange arrows.



1179  
 1180  
 1181  
 1182  
 1183  
 1184  
 1185

**Fig. 6a.** Monthly averaged ammonium wet deposition fluxes at nine EANET coastal sites (Figure 5). The black lines are three-year averages (2008-2010) of observations, and the blue lines are the corresponding model results. The vertical black lines represent the range of observed values for 2008-2010.



1186

1187 **Fig. 6b.** Same as Fig. 6a but for nitrate wet deposition fluxes.

1188

1189

1190

1191

1192

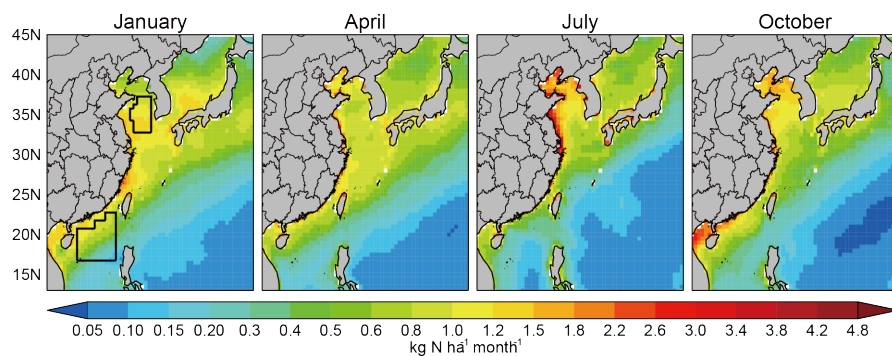
1193

1194

1195

1196

1197



1198

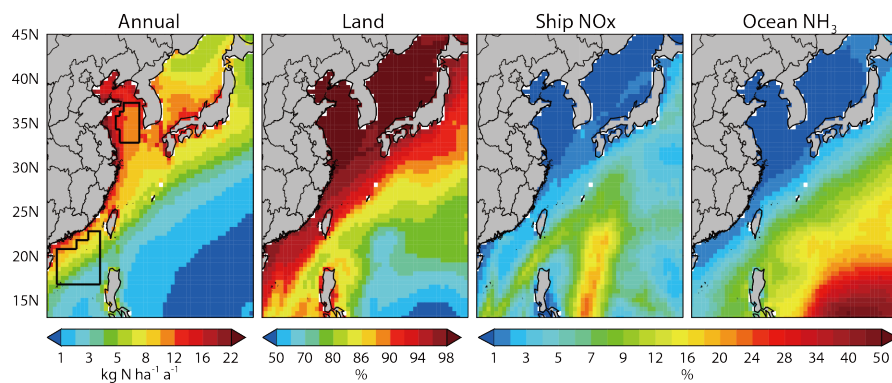
1199 **Fig. 7.** GEOS-Chem simulated monthly nitrogen deposition fluxes to the northwestern  
 1200 Pacific in January, April, July and October 2008-2010. The black boxes in the left  
 1201 panel represent areas of the Yellow Sea and the South China Sea used in the adjoint  
 1202 analyses.

1203

1204

1205

1206

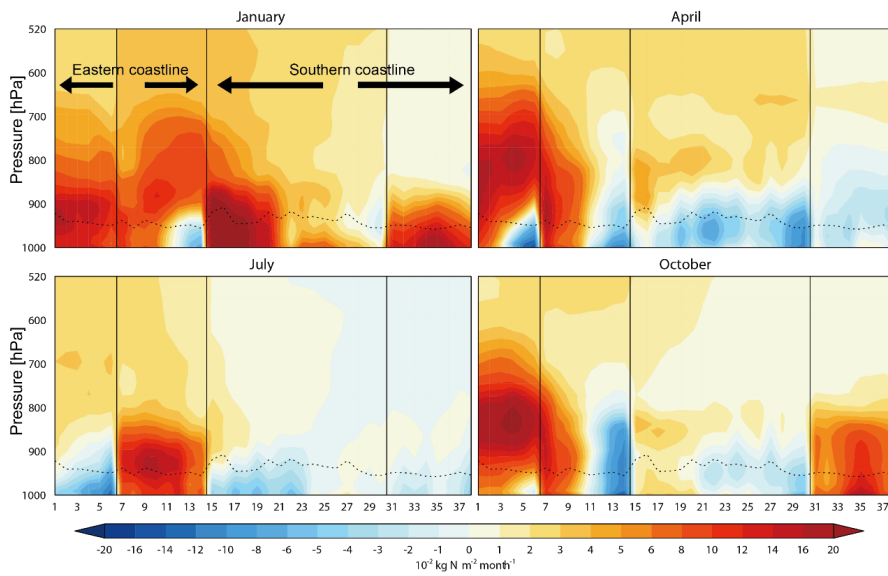


1207

1208 **Fig. 8.** Annual total nitrogen deposition fluxes to the northwestern Pacific averaged in  
 1209 2008-2010 (first panel), and annual percentage contributions from nitrogen sources  
 1210 over land, ship NO<sub>x</sub> emissions, and oceanic NH<sub>3</sub> emissions.

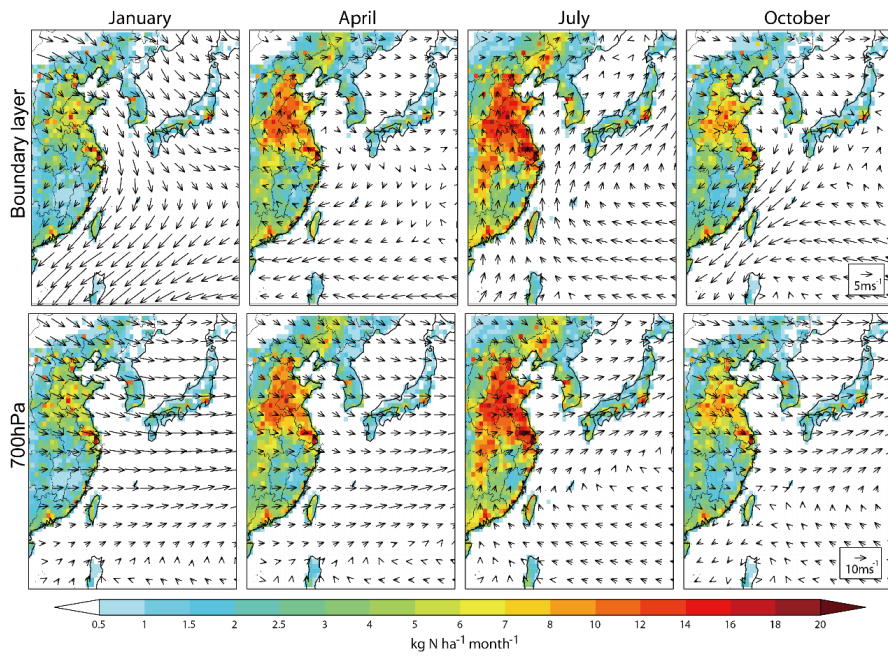
1211

1212



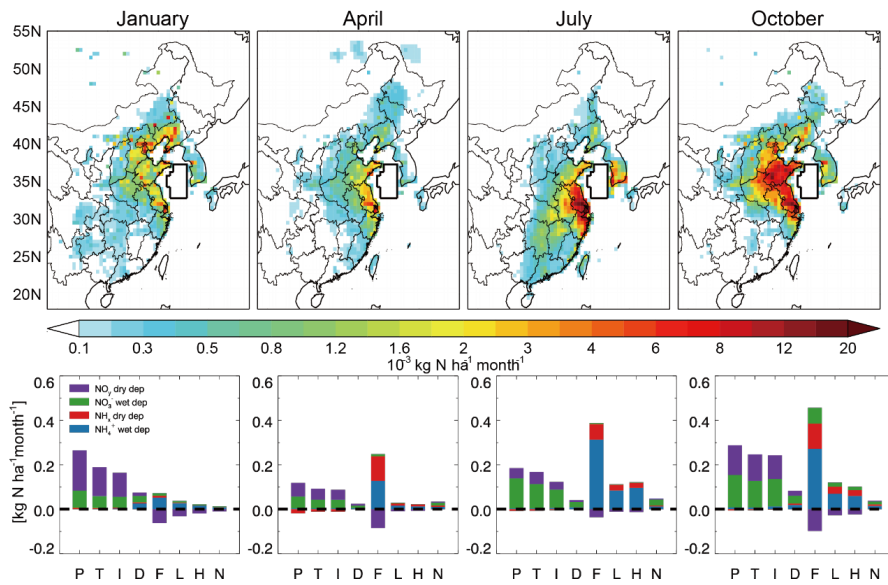
1213  
 1214  
 1215  
 1216  
 1217  
 1218  
 1219  
 1220  
 1221  
 1222  
 1223  
 1224

**Fig. 9.** Vertical profile of fixed nitrogen (totals of  $\text{NH}_3$ ,  $\text{NH}_4^+$ ,  $\text{HNO}_3$ , isoprene nitrates, and  $\text{NO}_3^-$ ) transported from the mainland of China to the ocean. The number of x-coordinate corresponds to the grid cell number in Figure 5. Positive values represent transport outside Mainland China, while negative values represent the opposite transport. The dotted lines represent the model boundary layer height. Three back lines divide the each panel in four parts. From left to right, we calculated transportation of nitrogen in each part in the direction of arrow F1 to arrow F4.



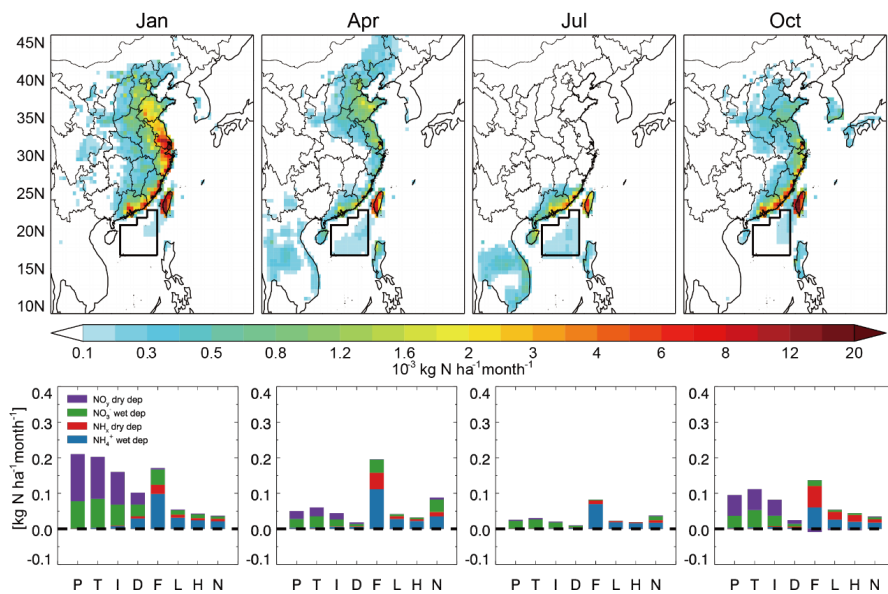
1225  
 1226  
 1227  
 1228  
 1229  
 1230  
 1231  
 1232  
 1233  
 1234

**Fig. 10.** Monthly mean wind fields from the GEOS-5 assimilated meteorological data over-plotted on the monthly emissions of fixed nitrogen ( $\text{NH}_3 + \text{NO}_x$ ). The top panels are wind fields in the boundary layer (1000 hPa-950 hPa) and the bottom panels show the wind fields in the free troposphere (700 hPa).



1235

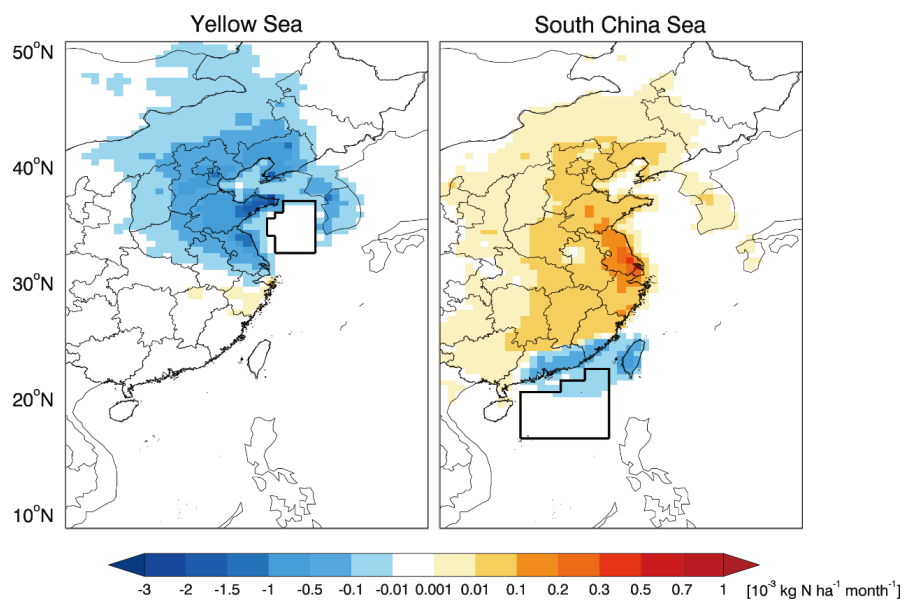
1236 **Fig. 11.** (Top panels) sensitivity of monthly total nitrogen deposition over the Yellow  
 1237 Sea to emissions in each grid box, and (bottom panels) sensitivity of nitrogen  
 1238 deposition over the Yellow sea (domain defined by the black lines) to each emission  
 1239 sector. In the x-axis labels P denotes Power plant, T: Transport, I: Industry, D:  
 1240 Domestic, F: Fertilizer use, L: Livestock, H: Human waste, and N: Natural emissions.  
 1241  
 1242



1243

1244 **Fig.12.** Same as Figure 11 but for the South China Sea.

1245  
1246



1247  
1248  
1249  
1250  
1251  
1252

**Fig. 13.** Sensitivity of  $\text{NO}_y$  dry deposition over the Yellow Sea (left) and over the South China Sea (right) to  $\text{NH}_3$  emissions in each model grid box for January 2009.